# LOW STRAIN PILE INTEGRITY TESTING FOR ROCK SOCKETED BORED PILES IN SRI LANKA

Thilina Hasantha Kodithuwakku

168964C

Degree of Master of Engineering

Department of Civil Engineering

University of Moratuwa
Sri Lanka

May 2020

# LOW STRAIN PILE INTEGRITY TESTING FOR ROCK SOCKETED BORED PILES IN SRI LANKA

Thilina Hasantha Kodithuwakku

168694C

Thesis submitted in partial fulfilment of the requirements for the degree

Master of Engineering

Department of Civil Engineering

University of Moratuwa

Sri Lanka

May 2020

## DECLARATION

I declare that this is my own work and this thesis does not incorporate without acknowledgement any material previously submitted for a degree or diploma in any other university or institute of higher learning and to the best of my knowledge and believe it does not contain any material previously published or written by another person except where the acknowledgement is made in the text.

Also, I hereby grant to University of Moratuwa the non-exclusive right to reproduce and distribute my thesis/dissertation, in whole or in part in print, electronic or other medium. I retain the right to use this content in whole or part in future works (such as articles or books).


…………………………………… Date:

Thilina Hasantha Kodithuwakku


The above candidate has carried out research for the Master's thesis under our supervision.


…………………………………… Date:

Prof. H.S Thilakasiri


…………………………………… Date:

Dr. L.I.N De Silva

## ABSTRACT

Low strain pile integrity testing has been available over several decades. It is the widely used method of pile testing to detect serious defects in piles. The transient dynamic response (TDR) method of low strain pile integrity testing needs pile top velocity and pile top force generated by a small handheld hammer hit. The velocity and force details are useful to estimate the pile condition near the top and the stiffness of pile-soil system

Researchers have proposed that dynamic stiffness at low frequencies associates to the static stiffness of pile head. The linear region of load-settlement behaviour of a pile is described by the static stiffness. However, little attention has been paid to developing a relationship between static stiffness and dynamic stiffness. The carrying capacity of pile is considered as the most important issue in pile foundations. Load Testing is the most reliable approach to evaluate the carrying capacity of piles. However, load tests are rarely performed as it is costly, labour intensive and time dependent, but all the piles are subjected to low strain integrity tests.

Following the testing results, this research proposes a relationship between dynamic stiffness and static stiffness of bored piles. It is intended to evaluate the allowable carrying capacity of piles with results of low strain pile integrity testing and high strength dynamic load testing. Finally, this research presents a simple methodology to estimate the allowable carrying capacity of piles using instrumented low strain pile integrity testing. The developed methodology will be verified using field load testing results. In addition to that, the success of implementing the TDR method on bored piles is proved by case studies.

**Key Words:** low strain pile integrity testing, high strain dynamic load testing, dynamic stiffness, transient dynamic response method, static stiffness, allowable carrying capacity, settlement, working load, mobilized load, PIT, PDA

# ACKNOWLEDGEMENTS

# TABLE OF CONTENTS

## LIST OF FIGURES

## LIST OF TABLES

# LIST OF ABBREVIATIONS

| Abbreviation | Description |
|---|---|
| CIDA | Construction Industry Development Authority |
| HSDT | High Strain Pile Integrity Testing |
| ICTAD | Institute of Construction Training and Development |
| LSPT | Low Strain Pile Integrity Testing |
| NDT | Non-Destructive Testing |
| PDA | Pile Driving Analyser |
| PIT | Pile Integrity Testing |
| PEM | Pulse Echo Method |
| TDR | Transient Dynamic Response Method |

# CHAPTER 1.    INTRODUCTION

## 1.1    Introduction

The constructions of mega structures are rapidly increasing due to the recent development of Sri Lanka. Most structures require deep foundation to transfer foundation loads to strong soil layers or rock layers. There are several types of piles used in Sri Lanka and the most common pile type is in – situ bored piles. Presence of strong bedrock formation at relatively shallow depth is a major factor for the wide spread use of in-situ piles. Ninety percent of Sri Lanka is built by highly crystalline, non-fossiliferous rocks of Precambrian age. Usually, piles are socketed one diameter (1D) length to five diameters (5D) in to bedrock based on design requirements and properties of bedrock. However, based on the investigations of load – settlement curves, it was concluded that 5% of the tested bored piles are faulty in Sri Lanka (H.S Thilakasiri, 2006). Thus, integrity issues of in-situ piles have created a significant need for economical Non-Destructive Testing (NDT) methods. NDT methods detects the extent and location of serious issues and avoid failures.

The most common testing method is pulse echo method from a hand held hammer, commonly referred as the pile integrity testing (PIT) in Sri Lanka.  In this method, the wave propagation induced by the hit of a hammer blow in the pile head is measured. The reflections of wave occur at the pile tip and also along the pile where the impedance of the pile changes. Changes in the pile can be occurred by variation of the cross section and/ or material properties.  Low strain pile integrity testing has advantages in terms of no advance preparation, low cost and easy use. Low strain pile integrity testing applies a different approach for interpretation of velocity and force measurements received from hammer blow. There are two main interpretation techniques used for low strain pile testing, the frequency domain analysis of velocity and force (TDR method) and the time domain analysis of pile top velocity (pulse echo method). Generally, pulse echo method is extensively used due to its direct relation to physical condition and ease of analysis.

In the time domain analysis, reflections from the pile axis where impedance changes and reflections from the pile toe are measured. The pile impedance is a function of elastic modulus (E), cross section (A) and wave velocity (c) and can be expressed as $Z = EA/c$. A pile that is long compared to diameter can be considered as a linear elastic pile which follows the one-dimensional wave propagation. An increasing in either elastic modulus or area makes a compressive reflection (reduction produces a tensile reflection). The transient dynamic response method needs a hammer with a load cell (instrumented hammer) to record the force impact and then, response signal can be evaluated. Velocity and force records are transformed to the domain of frequency and mobility plot. This TDR method differs from the pulse–echo method in that the frequency response of a pile is monitored for investigation rather than the propagation of stress wave in a pile.

The researches have proposed that dynamic stiffness of TDR method at initial frequencies relates to initial tangent of a load settlement curve received from a load test. According to Chan, H.F.C., 1987, a relationship between dynamic stiffness and static stiffness could be investigated by testing short model piles embedded in different soil types. Therefore, it is important to find a relationship between the static stiffness of combined pile-soil-rock system and the dynamic stiffness determined from the transient dynamic response method. This research suggests a relationship between the dynamic stiffness and static stiffness of bored and cast in-situ piles. The load-displacement behavior of piles in the initial linear zone of graph is expressed by the static stiffness. Furthermore, after load testing outcomes, this research proposes two settlement criterions as well. One criterion for linear zone of load-settlement graph and other criteria for non-linear zone of load-settlement graph. Pile elastic shortening and pile toe settlement are included in the derivations of these criterions. The allowable carrying capacity is restricted by the structural capacity, the geotechnical capacity or the settlement limit. Generally, good piles are failed by exceeding settlement limit or exceeding structural capacity. This research proposes a methodology to obtain the allowable carrying capacity of in-situ bored piles with the use of low strain pile integrity test results.

**1.2  Objectives of the research**

Specific objectives of this research are,

1.  Investigate the uses of transient dynamic response method for in-situ bored piles
2.  Develop a methodology to evaluate the allowable bearing capacity of in-situ bored piles with the use of low strain pile integrity testing

# CHAPTER 2.    REVIEW OF LITERATURE

Deep foundations are widely applied in Sri Lanka and in-situ bored piles are regularly used. Presence of strong bedrock formation at relatively shallow depth in most part of the country is the major factor for use of cast in-situ piles in Sri Lanka. Cast in-situ piles have some advantages over other type of piles. Low noise and vibration during installation and socketing are the main advantages of bored piles. The main disadvantage of bored piles is the construction difficulties which lead to many of the defective piles.  The performance of an in-situ pile foundation is influenced by the quality of construction. For quality assurance purposes, an NDT programme is generally conducted for a certain percentage of piles. Usually, the foundation engineer decides the piles to be tested based on site condition, judgment and experience.

## 2.1    Types of defects in piles

Concreting or tremie chock may cause specific integrity problems. Soil collapse, contamination of concrete, sudden changes in water table, delay in between arrival of two batches of concrete, improper extraction of temporary casing, improper flushing of pile bottom causing soft toe condition, and a variety of other reasons cause the defects in piles. Lack of technical skills or poor monitoring has also resulted in quality problems in piles.

According to the H.S Thilakasiri (2009), defects in the in-situ bored piles can be categorized in to two,

1. Defects affecting the geotechnical carrying capacity of piles
2. Defects affecting the structural carrying capacity of piles

### 2.1.1   Geotechnical carrying capacity of piles

Geotechnical carrying capacity of piles depends on end bearing and skin friction. Construction methods affect the development of end bearing and skin friction of piles. It is disputed that if the shear strength of the filter cake formed is more than that of the fluid concrete, it cannot be washed by the rising concrete surface during concreting, and filter cake can be left in the place. Then it leads to reduce the development of skin

friction. The pile bottom should be properly cleaned prior concreting; otherwise a layer of debris may be left in the toe. This soft toe condition leads to large settlements when the pile is loaded.

H.S. Thilakasiri (2006) investigated 67 load-settlement curves obtained from about 23 different sites across the country. Based on that investigation, it was concluded that about 5% of the in-situ piles are defective in Sri Lanka. The analysis of the load settlement curves and the site conditions of the defective piles indicated that the piles have undergone large plunging type settlements under very small end bearing resistance due to presence of relatively soft layer below the bottom of the pile.

### 2.1.2  Structural carrying capacity of piles

The cross section and the strength of concrete along the pile shaft play a major role in the structural capacity. According to the H.S Thilakasiri (2009), several reasons in reducing structural capacity are listed below.

1. Improper withdrawal of temporary casing causes reduction in cross section in concrete (necking)
2. Rising tremie pipe above the concrete level introduces horizontal slurry and mud intrusions.
3. Washing out of fines creates honeycombing
4. Collapsing of the side walls causes the contaminations and necking
5. Low – sump concrete creates voids

Reduction of cross-sectional area and weak concrete reduce the structural capacity of piles. Therefore Z (impedance) is expressed as given in Equation [2.1].

$$Z = A\sqrt{E\rho} \dots\dots\dots\dots\dots\dots\dots\dots\dots\dots\dots\dots\dots\dots\dots\dots\dots\dots\dots\dots\dots\dots\dots\dots\dots [2.1]$$

Where,

$A -$ cross section area

$E -$  elastic modulus of concrete pile

$\rho -$  density of the shaft

The intensity of the defect in terms of the parameter β is defined as $Z_2/Z_1$. Based on the value of β, defects can be classified as shown in Table 2.1.

Table 2.1 Intensity of the defects based on β (PDA User manual)

| $\beta = Z_2/Z_1$ | Damage assessment |
|---|---|
| 1.00 | Uniform |
| 0.80 – 1.00 | Slight damage |
| 0.60 – 0.80 | Damage |
| 0.60 > | Pile with a major discontinuity |

$Z_1$ – Nominal impedance of the pile shaft

$Z_2$ – Impedance of the defective pile section

## 2.2  Pile testing methods

Deep foundations integrity testing mostly applies to concrete foundations such as drilled shaft, auger cast piles, driven and cast in-situ piles etc. Depending on the site soil conditions, various methods are used to construct these foundations. It's very difficult to inspect and detect the pile quality by visual inspection as most piles are long enough. Integrity testing is a necessary requirement to control the quality after installation to find flaws in the piles that may have been caused to any of the above reasons. The design requirements of these foundations also require a high level of quality assurance and control. Currently the most commonly used method in the country to evaluate pile integrity is the Low-strain integrity test. But there are several other popular pile testing methods such as cross hole sonic logging testing, high strain dynamic load testing, maintenance load test etc.

### 2.2.1  Pile Integrity Test (Low Strain Integrity Test)

The Pile Integrity Test which has been available since the 1980s to indirectly determine the length and to search for large defects. This method has several advantages over other indirect methods, especially since it can be applied quickly to all precast concrete, bored shaft or auger cast-in-situ piles without much preparation. The changes of impedance at pile toe and pile axis produces reflections and those

reflections are measured in this test. The impedance depends on the speed of wave, elastic modulus, soil damping and cross section area. The induced wave reflections are used to detect changes of impedance and length of pile.

### 2.2.1.1   Pulse Echo Method (Time Domain Analysis)

One-dimensional wave propagation is applied in the pulse echo method. At some location, the impedance changes from $Z_1$ to $Z_2$ in the pile shaft. When Fi (downward travelling wave) reaches at this location, a portion of the wave is reflected up (Fu) and another portion propagates down (Fd) satisfying both equilibrium and continuity. The Equation 2.2 and Equation 2.3 can be obtained.  (Rausche and Goble, 1979).

$$F_d = F_i \frac{[2Z_2]}{[Z_2+Z_1]} \dots\dots\dots\dots\dots\dots\dots\dots\dots\dots\dots\dots\dots\dots\dots\dots\dots\dots\dots[2.2]$$

$$F_u = F_i \frac{[Z_2-Z_1]}{[Z_2+Z_1]} \dots\dots\dots\dots\dots\dots\dots\dots\dots\dots\dots\dots\dots\dots\dots\dots\dots\dots [2.3]$$

For a uniform pile, ($Z_2$=$Z_1$), neither the upward reflection $F_u$ nor the downward wave $F_d$ are produced and the input wave $F_i$ travels without changing. An example of extreme "nonuniformity" is a free pile end where $Z_2$ is zero. The downward wave will be fully reflected upward and Fu will have an opposite sign. Figure 2.1 shows that for a compressive downward travelling wave which encounters a cross – sectional reduction, an upward progressing tensile wave will be seen at the pile head at a time equal to two times the distance of disturbance divided by the wave speed.
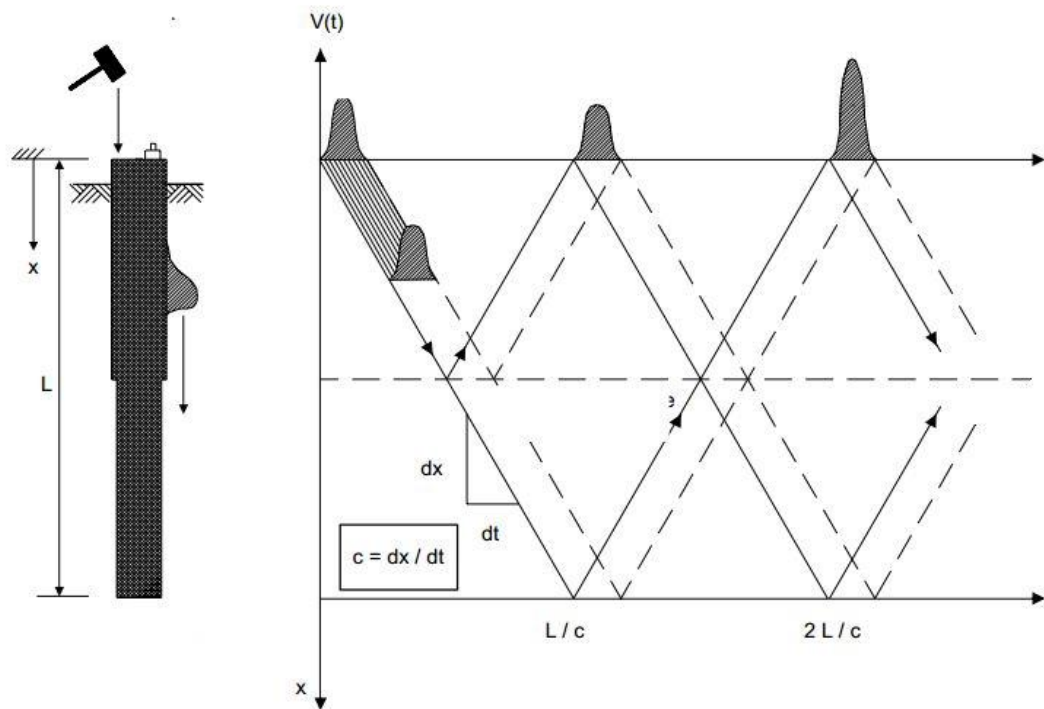
Figure 2.1 Velocity vs. Time signal

2.2.1.2　Frequency Domain Analysis (Transient Dynamic Response Method)

The arrival of fast spectral analyses accelerated the growth of the frequency domain NDT methods. The Transient dynamic response method needs the pile top motion and the impact force. Standard results of TDR method are a plot of the ratio of velocity to force (which is so – called Mobility) spectrum. The mobility is really the inverse of the impedance and therefore an indication of the pile's velocity response to a particular excitation force. The Fourier transformation on velocity and force signals can be performed to obtain the spectrum of force and velocity in the frequency domain. Distance to large defects and pile length may be received from distance between major peaks or patterns of the mobility plot. (PIT-W software manual). Figure 2.2 shows a typical record of TDR method.
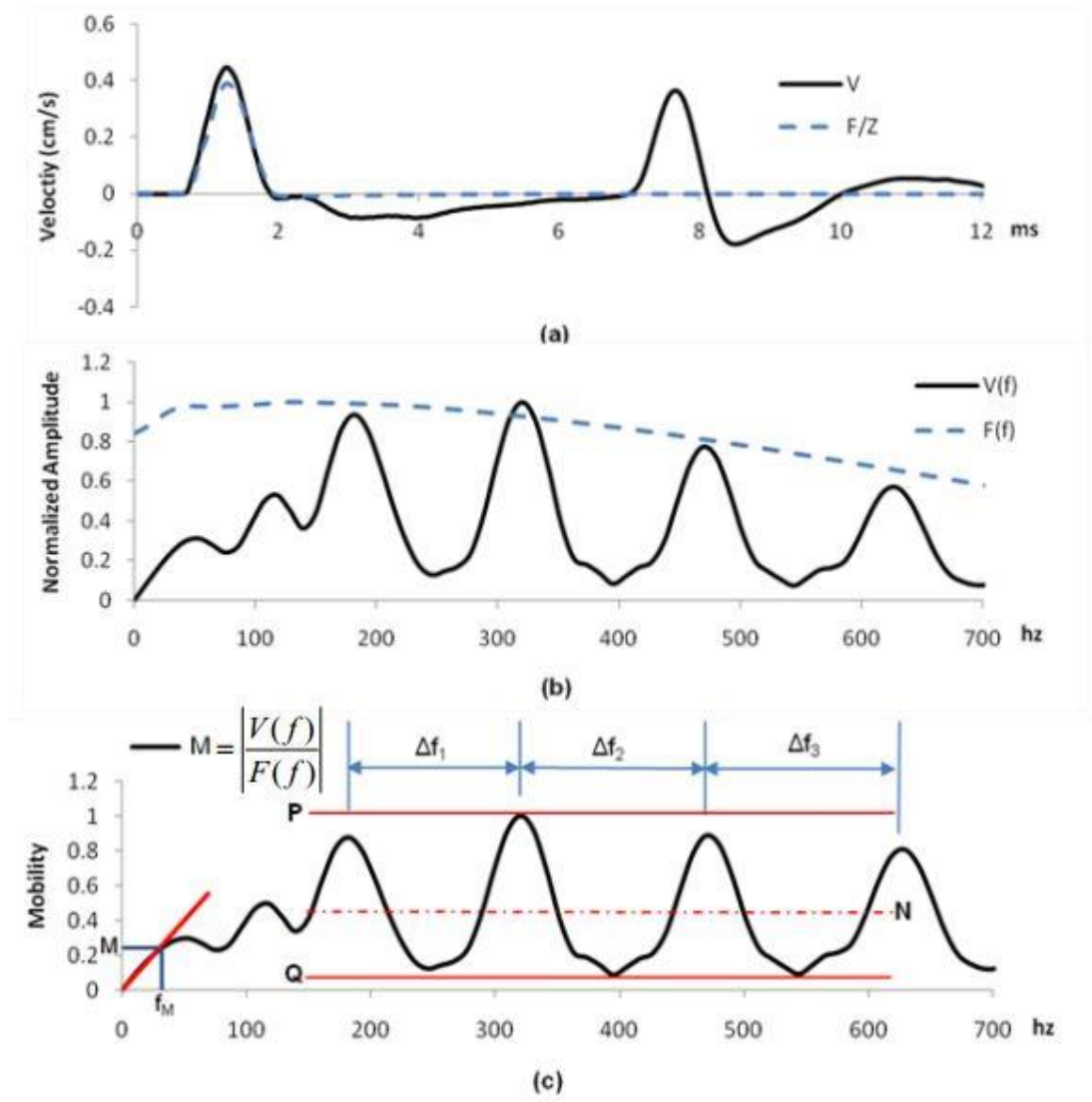
Figure 2.2 (a) Velocity and Force in Time Domain; (b) Spectrum of Velocity; (c) Mobility
(PIT-W user manual, 2009)

With the fast fourier transform of force and velocity measurements, the velocity, force, and mobility (velocity divided by force) curves are normalized against their maximum values within the range considered in frequency domain as observed in Figure 2.2, so that maximum point of each curve is 1.0. For the transient dynamic response method, the frequency content results from the repeating signals. A defect-free, long pile with high soil resistance may not indicate the toe reflections. Hence the signal will not repeat and frequency analysis would not work for length determination, but it may work to determine mobility and dynamic stiffness.

**2.3    ASTM Guidelines on interpretation and testing (Designation: D 5882 – 07)**

This test method covers recording and analyzing of force and velocity records of pile generated by an impact hammer.

**2.3.1    Procedure**

- Proceed with several impacts and records the measurements
- Conduct minimum three impacts and then average the selected records. Apply required amplifications.
- Integrity can be determined from averaged, amplified records.
- Integrity testing shall not be performed before 7 days of casting. The concrete strength shall be 75% of design strength.
- Clean the loose concrete and other debris to ensure a sound pile head surface. If necessary, remove a part of pile head to reach the sound concrete.
- I needed, provide a smooth finish to pile top by a grinder
- Motions sensors need to be attached firmly at specified location but away from edge.
- Use minimum of three location for accelerometer attachment for piles larger than 500 mm in diameter.
- Accelerometer and impact should be in distance less than 300 mm
- Final evaluation regarding integrity should be done by an experienced engineer

**2.3.2    Signal treatment**

- The accelerometer's analog output is first converted to a digital signal
- The software (PIT-W) must go through the following operation to transform raw data into a reliable reflectograms

| Operation | Description |
|---|---|
| Integration | Input transformed from accelerometer to velocity |
| Filtering | To receive a smooth graph, eliminating low frequency noise and high frequency noise |

| Rotation | Rotate the curve to reduce the enclosed area between curve and horizontal axis |
|---|---|
| Amplification | Amplify the stress wave exponentially |

## 2.4    Low strain pile integrity test - Interpretation

One - dimensional wave propagation across the pile is assumed for interpretation of the small strain dynamic test. The main assumptions are.

- The wave length of the propagating wave is larger than the diameter of the pile tested
- The velocity of the wave is independent of the frequency (wave is non-dispersive)
- No attenuation of the propagating wave occurs due to leakage of energy from the shaft to the surrounding soil
- The reflected waves are generated only at the changes in the shaft geometry or properties, at the toe of the pile, and at the relatively high stiffness variation of the layers present along the pile shaft
- No scattering effect of the stress wave due to the changes of the pile material's properties.

Proper understanding of sign convention used in the velocity and the force is very important for analysis of the integrity test results. Relationship between the directions of the wave propagating and the particle velocity should be understood for successful interpretation. Compression forces or tension forces can be generated along the direction of propagation of the wave. Relationship between the direction of the wave and the direction of particle velocity for compression and tension waves is shown in the following Figure 2.3.

### 2.4.1    Pulse echo method

The zero point where we begin recording time shall be decided for a good interpretation. Usually hammer impact completed within one to two milliseconds. Therefore, the zero point should be defined. This option shall be permanent and

assigned to all reflections. As shown in the following Figure 2.4, point A (where pile head start to move) or point B (where maximum point of the initial blow) can be taken.





(a) Compression wave                                    (b) Tension wave

 Direction of the wave propagation     Direction of the particle velocity
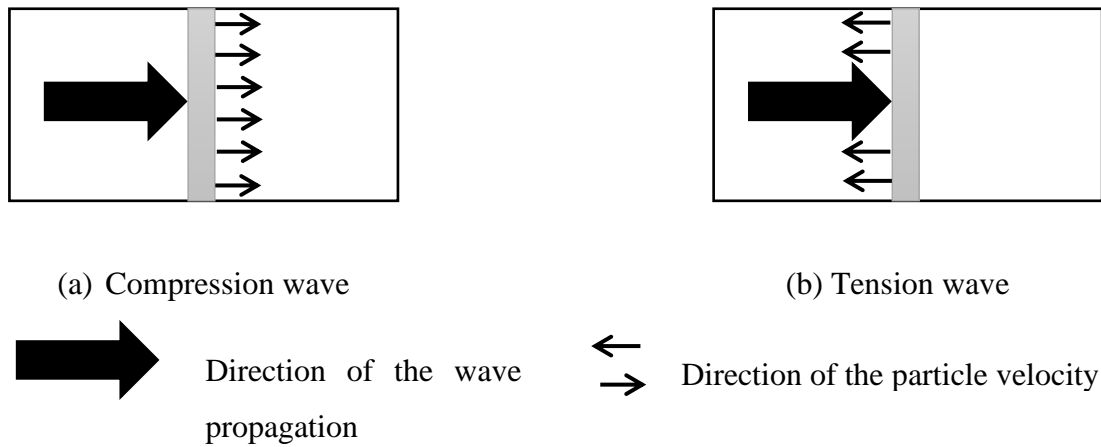
Figure 2.3 Relationship between direction of the wave velocity and the particle velocity

In the time domain analysis or pulse echo method (PEM), pile top velocity is analysed in the time domain. PEM gives stuffiest details for integrity determination. Pile top velocity vs depth curve is used to display the test results. The American application is to place the first hammer impact upwards, while the European prefers to show it downwards. Figure 2.4 shows the American and European practices. Quantitative interpretation is the first step in analysing the reflectgram. Quantitative interpretation can be conducted instantly after every test. Comparing the graph can be done mentally with the use of various pile shapes and respective reflectograms (Rausche et. al 1988). Refer Table 2.2.
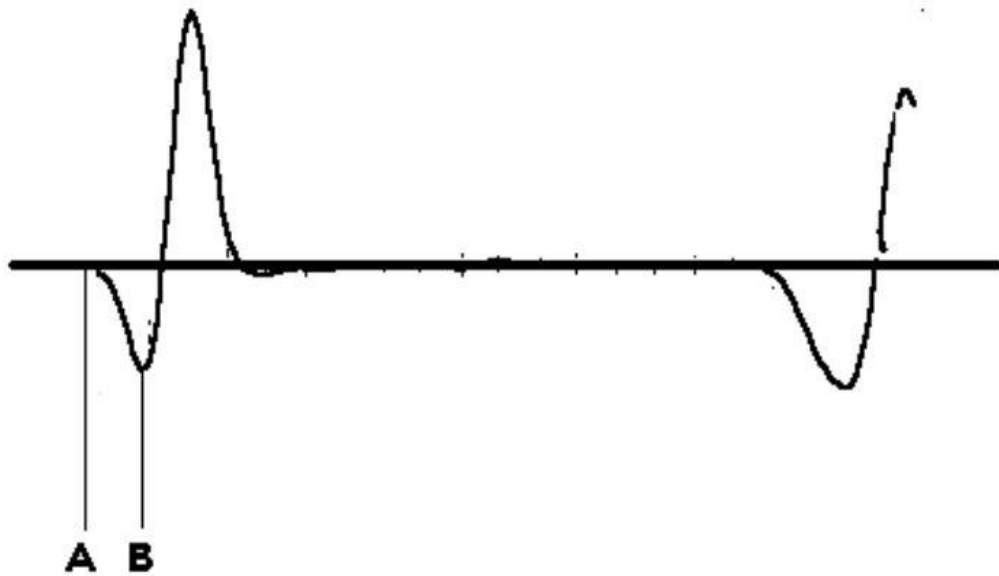
Figure 2.4 Alternative points for zero point

## 2.4.1.1 Effect of Skin Friction on the reflectograms

The stress wave traveling through the pile tends to move the particles of the pile relative to the surrounding soil. Then a resistant force is developed by surrounding soil against the movement of the particles of the pile. Impedance may be considered as the resistance offered by the pile section against the particle velocity. Larger piles and stiff pile materials offer higher resistance against particle movement. Where higher skin friction is acting can be considered as sections with higher impedance. Reflections due to soil resistance should be separated for clear reflectograms. Reduction of the magnitude and energy of the propagation wave due to impedance variation and soil resistance is the major problem. So, identification of the defects at deeper levels from the reflected waves is very difficult. The particle velocity of a pile with minimum soil resistance and minimum pile resistance measured at pile top is illustrated in Figure 2.6. And particle velocity of a pile with soil resistance and minimum pile resistance measured at the pile top is illustrated in Figure 2.7.
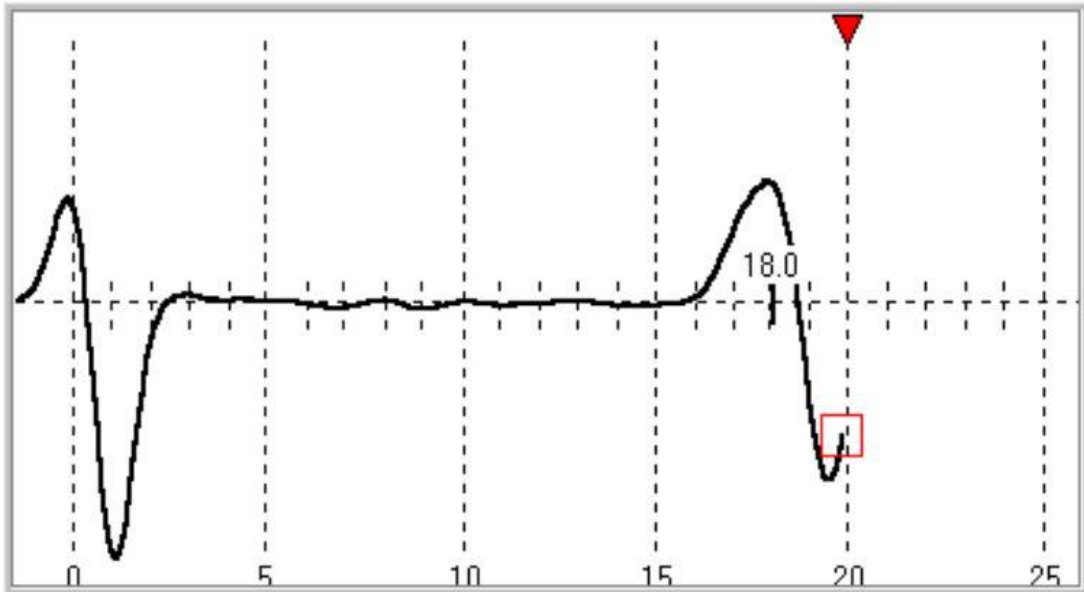
a)  American method
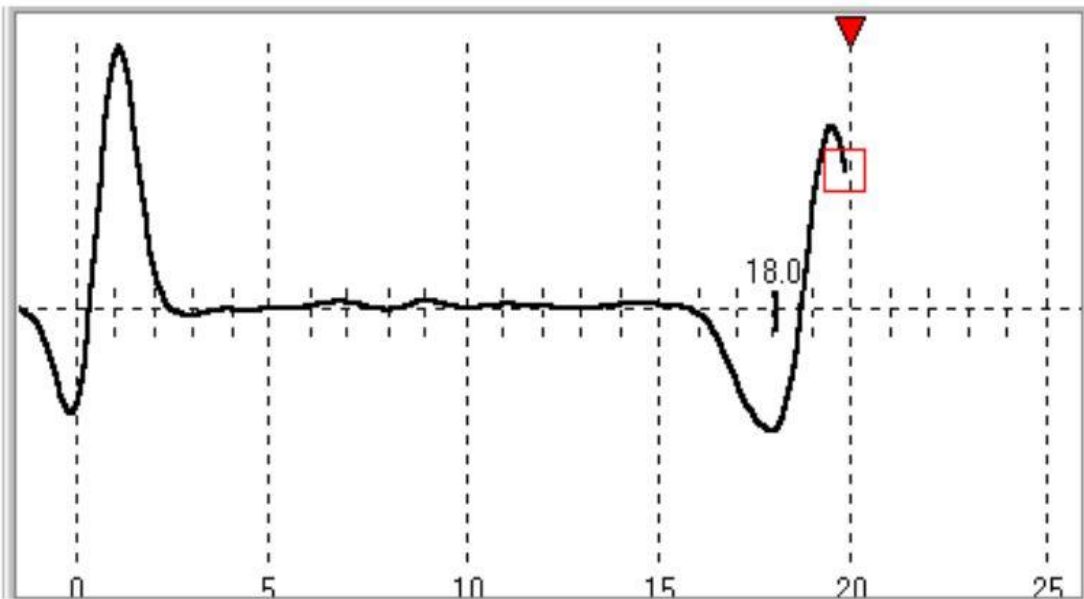


b)  European method

Figure 2.5 American and European practices (Pile integrity testing, 2009)
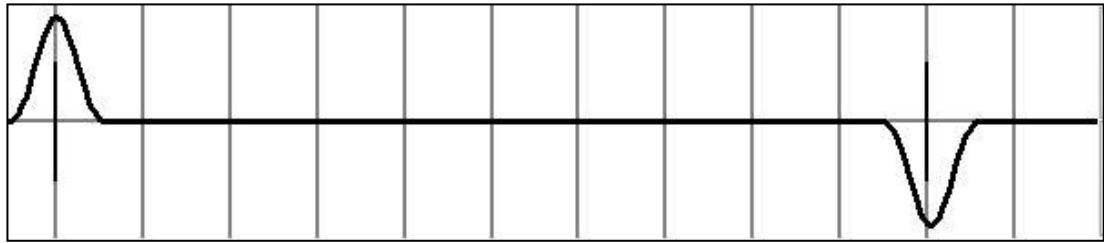
Figure 2.6 The particle velocity of a pile with minimum soil resistance and minimum pile resistance measured at the pile top
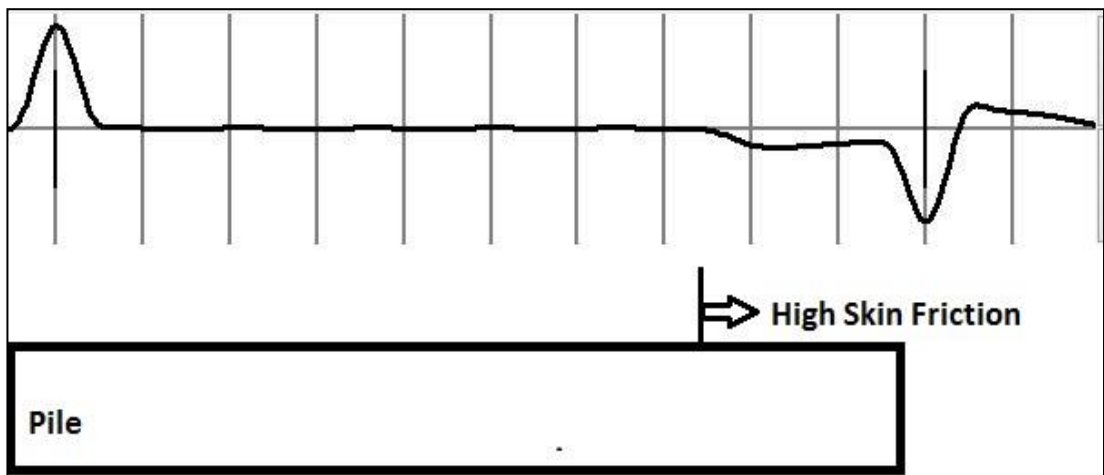


Figure 2.7 The particle velocity of a pile with soil resistance and minimum pile resistance measured at the pile top

2.4.1.2  Damage detection

The compression wave velocity (c) through semi – infinite elastic medium is given by Equation [2.4].  The compression wave speed is independent of Poisson's ratio for piles with diameter much less than the wave length.  Therefore, one dimensional compression wave velocity through a pile can be expressed in Equation [2.5].

$$c \;=\; \sqrt{\frac{E(1-v)}{\rho(1+v)(1-2v)}} \qquad \text{………………………..…………………………………...} \quad [2.4]$$
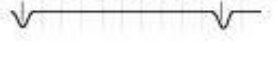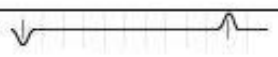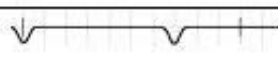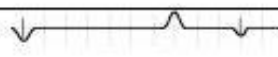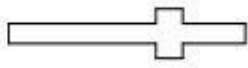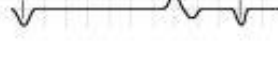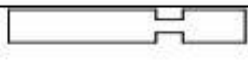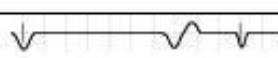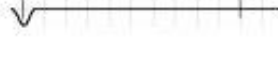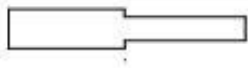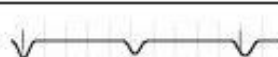
$$c \;=\; \sqrt{\frac{E}{\rho}} \qquad \text{………………………………………………….………………} \quad [2.5]$$

The toe reflection is visible in the velocity record $\frac{2L}{c}$ after the velocity pulse due to the initial impact.

Similarly, the relationship between the time (t) and the depth (L) to the location of the anomy in the pile shaft is given in Equation [2.6].

$$L = c\frac{t}{2} \dots\dots\dots\dots\dots\dots\dots\dots\dots\dots\dots\dots\dots\dots\dots\dots\dots\dots\dots\dots\dots\dots\dots\dots [2.6]$$

Table 2.2 Typical piles with respective reflectrogram reflectograms  (Rausche et. al 1988)

| | | |
|---|---|---|
| | Straight pile, | |
| | Straight pile, | |
| | Straight pile, | |
| | Increased | |
| | Decreased | |
| | Locally | |
| | Locally | |
| | High L/D ratio | |
| | Multiple reflections from | |
| | Irregular profile | |

### 2.4.2   Transient Dynamic Response [TDR] method

The transient dynamic response method needs measuring the force and velocity at pile top. The combination of velocity and force can provide extra details about the pile condition. The TDR method needs a hammer with load cell to record the force.  Then velocity and force signals are turned to the frequency domain and mobility plot. The mobility is the inverse of impedance.

2.4.2.1   Length measurements

Length readings are determined from the distance between resonance peaks resulted from toe or anomalies. In frequency domain, defect location or pile length can be determined by Equation [2.7].

$$L = \frac{c}{2 \times \Delta f}$$ …………………………………………………...…………………. [2.7]

Where

L - Distance from the gage to a defect or pile toe (m)

$\Delta f$ - Frequency difference between peaks of mobility curve or velocity spectrum (H$_z$)

c- Wave speed (m/s)

2.4.2.2   Dynamic Stiffness

The pile top response to impact is usually linear at low frequencies. At low frequencies the pile unit moves as one unit. Therefore, dynamic stiffness is calculated at low frequencies only. Dynamic stiffness can be determined by Equation [2.8].

$$K_d = \frac{2\pi f_M}{M}$$…………………………………………………………….…… [2.8]

Where,

$f_M$ − Any frequency close to origin where the mobility plot is linear

$M$ − Mobility value for the $f_M$

The dynamic stiffness relates to the elastically recoverable spring stiffness of the pile. It can be compared to$\frac{EA}{L}$. Higher dynamic stiffness may indicate a bulge or higher shaft resistance. While lower value may indicate a defective pile or a lower shaft resistance (PIT – W software manual).

### 2.4.2.3   Measurement of Mobility

The theoretical mean value of mobility in the stable zone of mobility graph can be expressed as given in Equation [2.9].

$$N_c = \frac{1}{\rho c A}\dots\dots\dots\dots\dots\dots\dots\dots\dots\dots\dots\dots\dots\dots\dots\dots\dots\dots\text{ [2.9]}$$

Where,

$\rho$ – density of pile material $(kg/m^3)$

$c$ – wave speed $(m/s)$.

$A$ – pile cross section $(m^2)$

Measured mean value of mobility shall be expressed by its geometric average as given in Equation [2.10].

$$N_m = \sqrt{PQ}\dots\dots\dots\dots\dots\dots\dots\dots\dots\dots\dots\dots\dots\dots\dots\dots\dots\text{ [2.10]}$$

Where,

$P$ – Highest peak mobility value $(m/Ns)$

$Q$ – Lowest valley mobility value $(m/Ns)$

$N_c$ and $N_m$ are closed to each other for a uniform pile. Typically, $N_m$ lies between 0.5 and 2.0 of $N_c$. the pile might be defective, if $N_m$ is larger than $N_c$ and $K_d$ lower. If $N_m$ is less than $N_c$ and $K_d$ is higher, the pile may have bulges (PIT – W software manual).

Simulation of measured velocity and force of a typical pile is expressed in the Figure 2.8.
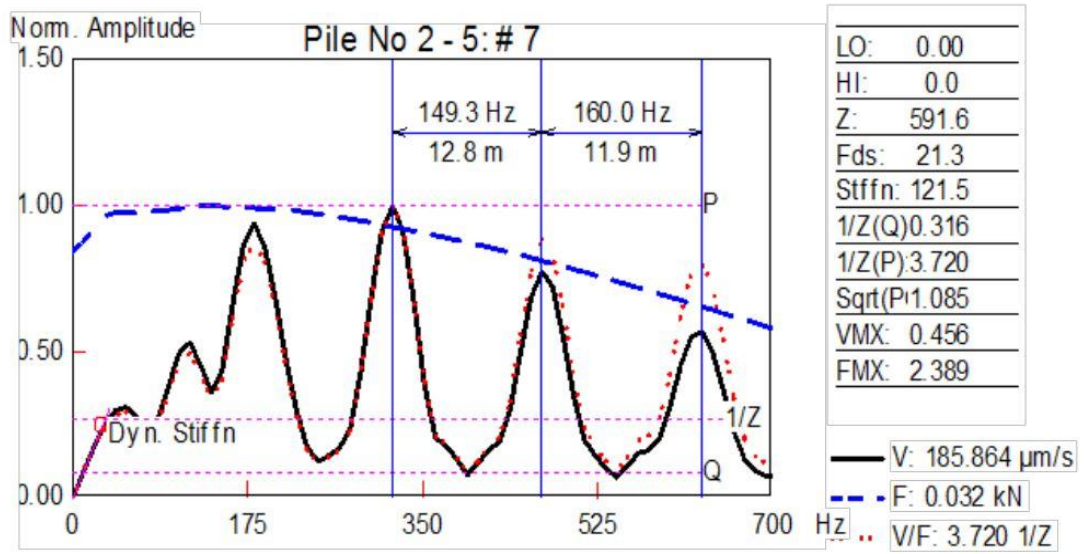
Figure 2.8 Simulation of measured velocity and force of a typical pile (PIT – W
software manual)

# CHAPTER 3.    METHODOLOGY

## 3.1    Developing a correlation for the static stiffens from the dynamic stiffness and investigate the uses of TDR method

Well-ordered site tests were conducted on in-situ piles in Sri Lanka. Field testing was carried out using both low-strain pile testing (commonly referred as PIT) and high-strain dynamic testing (commonly referred as PDA). Tested piles bored in the soils in low lands (mostly soft peaty soils) and socketed in to the bedrock strata. The piles were 600mm to 1800mm in diameter, 7m to 50m in length and with 1 diameter to 5 diameters socket length. Low-strain pile integrity testing was conducted as described in the ASTM D 5882 – 07. A 5.45 kg impact hammer instrumented with a load cell was used to impact the pile top, and velocity records were obtained with a high-sensitivity accelerometer attached to the pile top. Force and velocity measurements taken through LSPT were analysed in both time domain and frequency domain to investigate the transient response of the pile. The data was analysed to determine the dynamic stiffness ($K_d$) from frequency analysis using the PIT-W$^{TM}$ software.

High-strain dynamic load testing was conducted as described in ASTM D 4945. The field measurements were recorded with the pile driving analyzer (PDA$^{TM}$). In order to simulate the static load – displacement response of bored piles, the processed data were analysed from the CAPWAP$^{TM}$ software using signal-matching technique. The quality of the signal match was maintained by requiring a Match Quality value (MQ) less than 5. The initial linear regions of load – settlement curves (one for top and one for toe of pile P2) are shown in Figures 3.1 and 3.2 respectively. Finally, initial linear regions of load – settlement curves were used to determine static stiffness at the top ($K_{top} = 273.12$ MN/m) and at the toe ($K_{toe} = 145.56$ MN/m).

Dynamic stiffness from the LSDT plotted against the static stiffness from the HSDT to determine their relationship. Thereafter, a correlation between $K_d$ and $K_{top}$ was suggested to estimate the static stiffness (K) using the dynamic stiffness ($K_d$). In addition to that, the pile top settlement under the working load was calculated using suggested K and compared with the pile-top settlement determined through static-response simulation of HSDT. The static stiffness value (K) was also compared with

the value of EA/L, and the base fixity of the piles was investigated using the first resonant frequency. Finally, the effective length of pile was discussed in time domain and frequency domain.
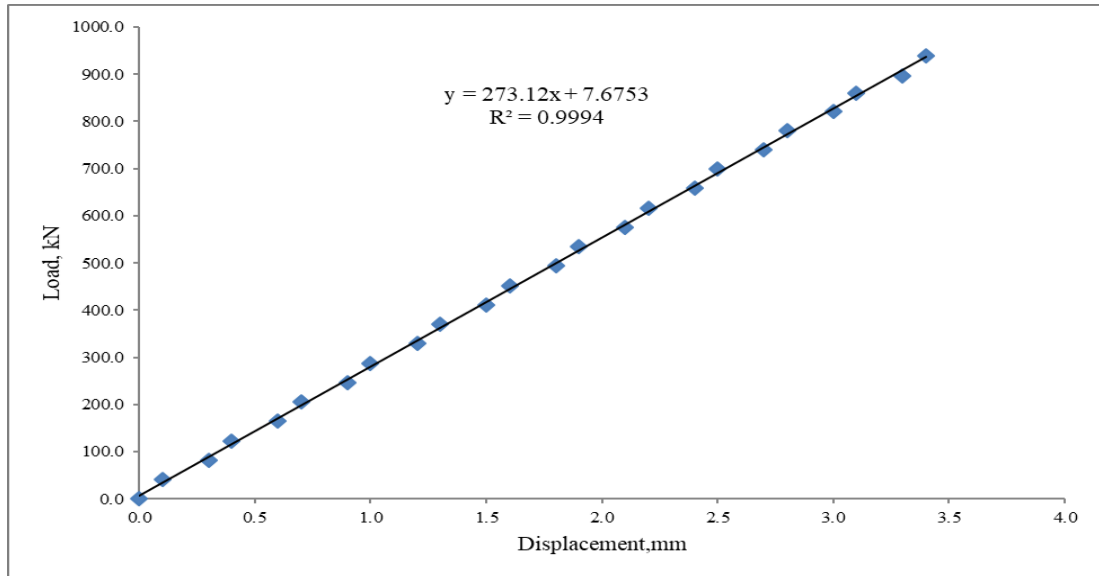


Figure 3.1 Load - settlement curve at the top
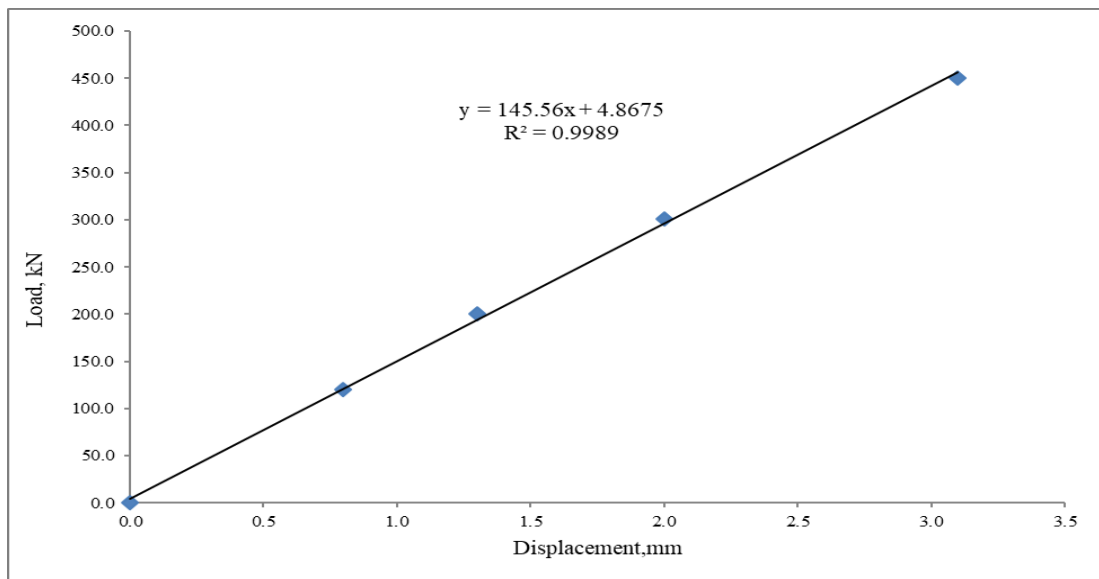


Figure 3.2  Load - settlement curve at the bottom

## 3.2 Developing a methodology to determine the allowable bearing capacity of bored piles using low strain pile integrity testing

The pile toe displacement subtracted from pile head displacement to obtain the pile elastic shortening under any load of high strain load testing results. The interpreted shortening can be expressed as PL/AE (P=load at pile head, L= length of pile, A=cross sectional area). Two sets of piles were used to estimate the elastic shortening and interpreted shortening. One set of piles has reached only up to the linear region of load settlement curve and other set of piles has reached the non-linear region of load settlement curve as well. Then, measured pile elastic shortening plotted against the interpreted shortening in the linear and the non-linear regions to estimate their correlations. Later, a correlation for the pile toe stiffness, $K_{toe}$. is developed.

Furthermore, two settlement criterions for linear and non-linear regions of load-settlement graph are proposed. As outlined in ICTAD (CIDA), A 12mm settlement is allowed under the working load. It is conservatively assumed that the maximum allowable bearing capacity always reaches to the non-linear zone of load settlement graph. If the pile exhibits higher settlements than the specified settlement limit with allowable structural capacity, the corresponding load to the allowable settlement limit is taken as the allowable carrying capacity. And if the observed pile settlement is less than the settlement limit when loaded to structural capacity, the structural capacity is considered as the maximum allowable bearing capacity of pile.

### 3.2.1 Settlement Criterions for Piles

There are two parts in the vertical settlement of a pile namely pile toe displacement and the pile axis elastic shortening. The elastic shortening can be taken as PL/AE only if there is no friction resistance along pile. But, generally value of elastic shortening is less than the PL/AE due the skin friction along the pile shaft. Therefore, elastic shortening is considered as αPL/AE. The α is less than unity.

The elastic shortening in the both regions of load-displacement graph were investigated as listed below in the section 4.21. and 4.22 respectively. The two regions of general load-displacement graph are shown in Figure 3.3. Calculations for the pile toe stiffness and pile toe load are listed in section 4.2.3. The pile toe stiffness and the pile toe load can be used to estimate the pile toe displacements. The suggested criterion for the estimation of settlement is expressed as shown in Eq. 3.1.

$$\Delta = \ \alpha \frac{P_{top}L}{AE} + \frac{P_{toe}}{K_{toe}} \dots\dots\dots\dots\dots\dots\dots\dots\dots\dots\dots\dots\dots\dots\dots\dots\dots\dots\dots\dots (3.1)$$

$\Delta = $ Pile top displacement for the pile top load

$\alpha - $ Constant

$P_{top} - $ pile top load

$P_{toe} - $ pile toe load

$K_{toe} - $ Stiffness of pile toe

$L - $ Length of pile

$A - $ Cross sectional area of pile

$E - $ Concrete elastic modulus
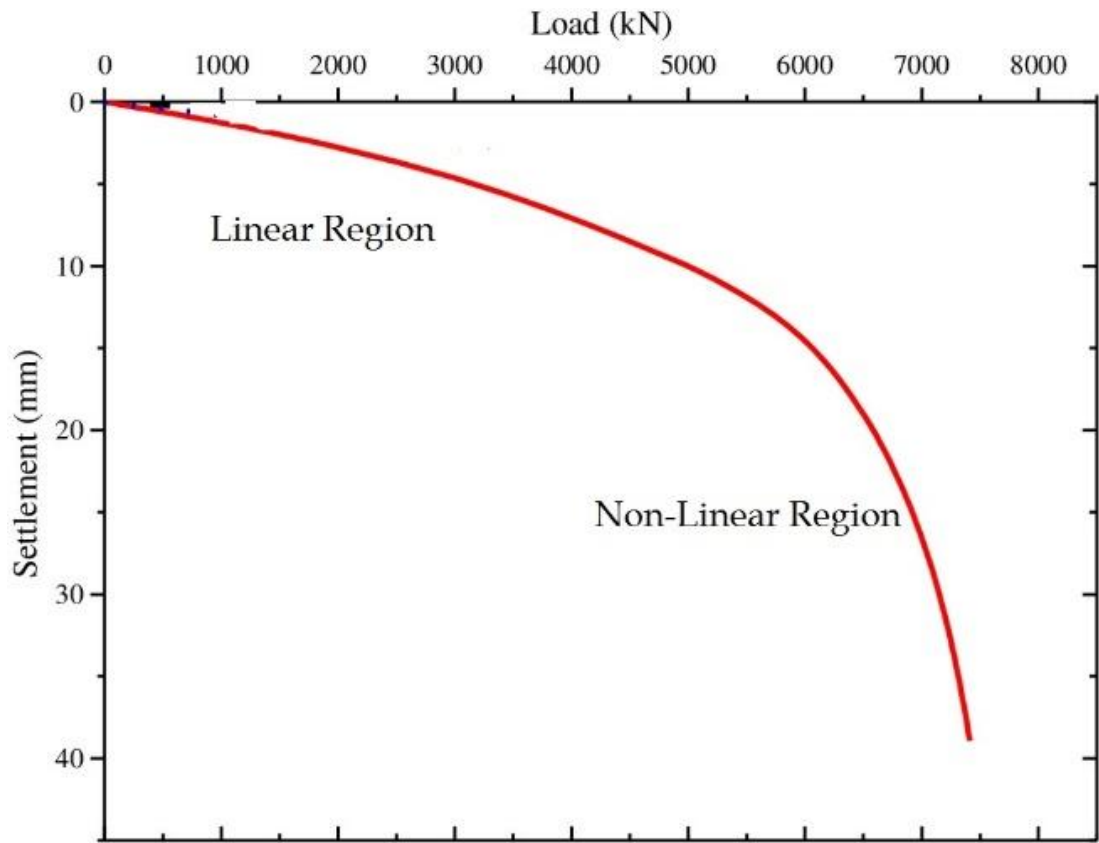
Figure 3.3 Load-Settlement Curve

# CHAPTER 4.    RESULTS AND DATA ANALYSIS

## 4.1    Developing a correlation for the static stiffens from the dynamic stiffness and investigate the uses of TDR method

### 4.1.1    Dynamic Stiffness ($K_d$)

Static stiffness calculated from the signal-matching analysis plotted against dynamic stiffness calculated from TDR method is displayed in Figure 4.1, and the results are listed in Table 4.1. As shown in the Figure 4.1, a linear curve with a coefficient of determination of 0.80 matches the data well. Therefore, the static stiffness shall be obtained from dynamic stiffness with a reasonable accuracy. The correlation (Eq 4.1) will be used to obtain static stiffness through the dynamic stiffness.

$$\text{Static stiffness (K)} = 1.082 \times \text{Dynamic Stiffness}(K_d) + 7.151 \dots\dots\dots\dots\dots\dots (4.1)$$

Under the working load, the piles are generally in initial linear zone of the load – settlement curve. Thus, the dynamic stiffness value together with this correlation can be used to calculate the load – displacement behavior of a pile under the working load. However, the user's experience with testing and analyzing is crucial for clear and quality test results. Settlement ($\delta$) under the working load was calculated by using the static stiffness (K) as indicated in Eq 4.2, and the settlement under working load was determined from the static simulation of HSDT. The settlement difference ($\Delta\delta$) and percentage of settlement difference of the two testing methods, HSDT and LSPT, were calculated as indicated in Eqs 4.3 and 4.4. Settlement calculation for the tested piles under the working load (WL) is listed in Table 4.2 with the estimated maximum settlement difference and the percentage of settlement difference. Estimated maximum settlement difference and percentage of settlement difference were in the range of -1.1mm to +2.5mm and -53% to +41% respectively as indicated in Table 4.2.

$$\delta = \frac{WL}{K} \dots\dots\dots\dots\dots\dots\dots\dots\dots\dots\dots\dots\dots\dots\dots\dots\dots\dots\dots\dots\dots\dots\dots\dots\dots\dots\dots\dots\dots (4.2)$$

$$\Delta\delta = \text{ LSPT } \delta - \text{HSDT } \delta \dots\dots\dots\dots\dots\dots\dots\dots\dots\dots\dots\dots.\dots\dots\dots\dots\dots\dots\dots.. (4.3)$$

$$\text{Percentange } \Delta\delta = \frac{\Delta\delta}{\text{HSDT } \delta} \times 100 \% \dots\dots\dots\dots\dots\dots\dots\dots.\dots\dots\dots\dots\dots\dots\dots\dots (4.4)$$
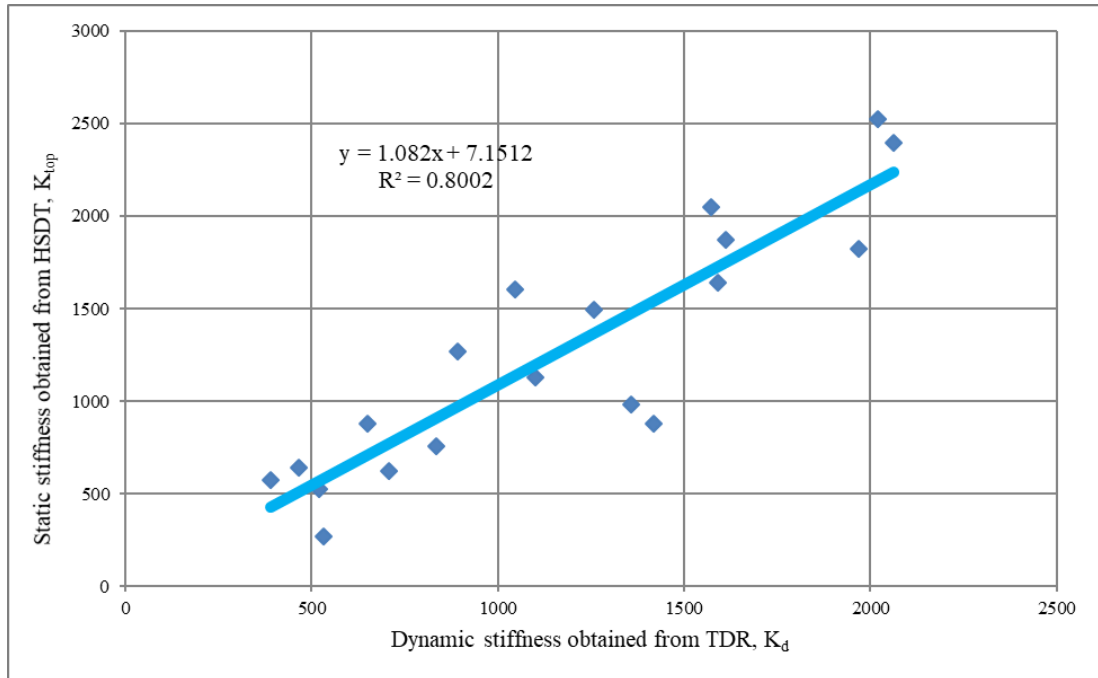
Figure 4.1 Static stiffness of pile head vs. dynamic stiffness of pile head

Results obtained for 1,800 mm diameter piles through the LSPT were inconsistent, and it was almost impossible to determine the dynamic stiffness of piles due to non-linearity of the mobility plot close to the zero frequency. In large piles, force and velocity is not proportional due to limited spherical point contact of impact. It was observed that dynamic stiffness of large-diameter piles varies widely depending on the location of the hammer hit and the corresponding force on the pile top. Thus, dynamic stiffness calculations may not be meaningful for large-diameter piles. However, reliable results were obtained up to a diameter size of 1,500 mm. P17 is a 1500mm diameter pile that has an irregular shape as observed in time-domain reflectogram (Figure 4.2). Although, it is difficult to interpret the peak pattern of the mobility plot, a linear region of the mobility is observed close to the zero frequency as shown in Figure 4.2. Thus, pile P17 yielded a reliable dynamic stiffness value of 2,018.5 MN/m, which agrees well with static stiffness of 2,523.8 MN/m (Table 4.1) obtained from HSDT.

The response spectrum of the 21.63m-long pile P6 with a peak pattern corresponding to 5.8m length yields a dynamics stiffness of 519.7 MN/m (Figure 4.3), which has a good agreement with the stiffness of 526.3 MN/m from HSDT stiffness (Table 4.1).

The anomaly at 5.8m depth can be identified as a bulging which extends from depth of 5.8m depth as observed in time domain reflectogram (Figure 4.3). In this case, depth to the bulging can be estimated, but not the overall length. It can be seen that some skin friction may have developed along the pile length, approximately from 14m to 18m depth as observed in time-domain reflectogram (Figure 4.3). Thus, some of stress waves may have passed through the bulging region and travelled to a certain depth of the pile. Therefore, dynamic stiffness calculated from this mobility plot could be meaningful. However, it's doubtful that dynamic stiffness is meaningful when the peak pattern indicates depth to the major anomaly instead of total pile length. In such instances, advanced methods would be needed to obtain a reliable static stiffness.
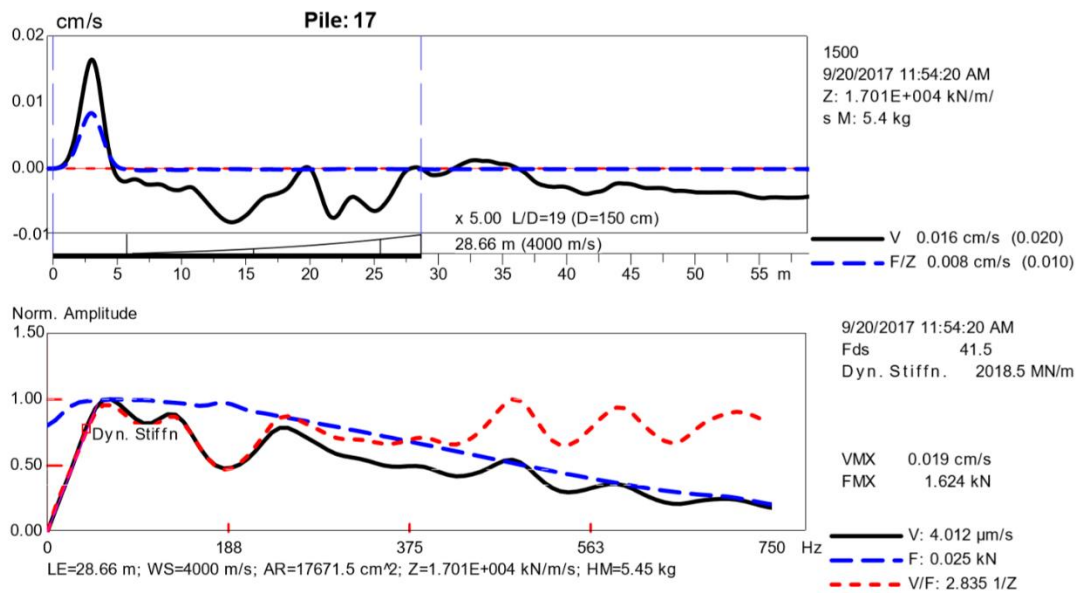


Figure 4.2 Time domain reflectogram and mobility spectrum of pile P17
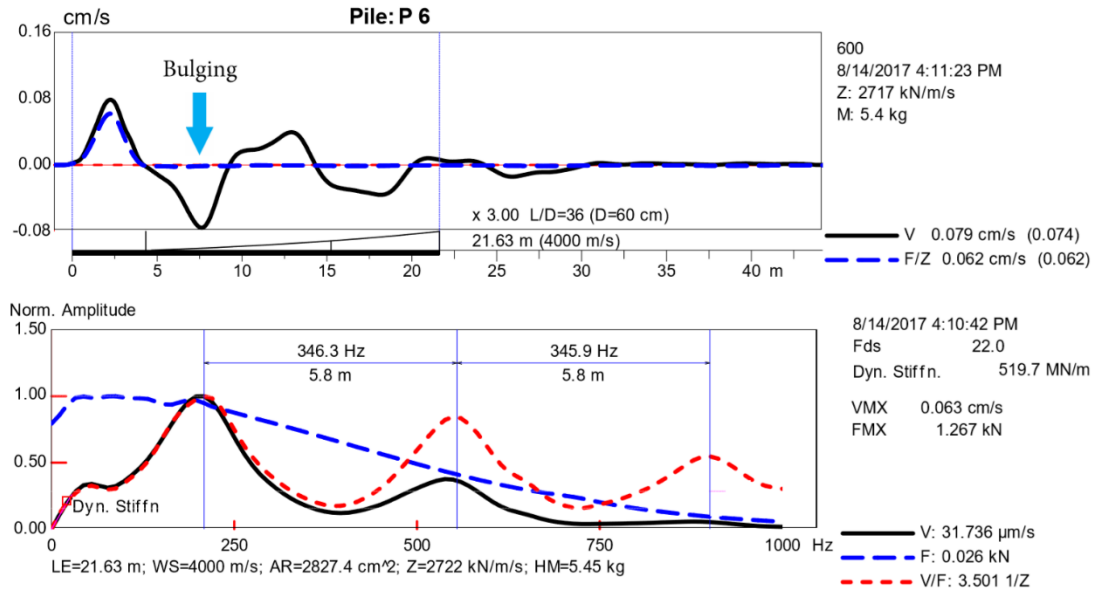
Figure 4.3 Time domain reflectogram and mobility spectrum of pile P6

Table 4.1 List of pile stiffnesses determined from TDR and HSDT methods

| Pile ID | Diameter, mm | Length, m | $K_{top}$, MN/m | $K_d$, MN/m |
|---------|--------------|-----------|-----------------|-------------|
| P1 | 1000 | 21.4 | 881.0 | 1418.0 |
| P2 | 800 | 8.3 | 273.1 | 531.8 |
| P3 | 600 | 7.3 | 640.2 | 467.0 |
| P4 | 800 | 19.0 | 982.9 | 1,358.7 |
| P5 | 750 | 23.0 | 573.4 | 389.2 |
| P6 | 600 | 21.6 | 526.3 | 519.7 |
| P7 | 1,500 | 16.1 | 1,870.7 | 1,610.5 |
| P8 | 1,500 | 22.7 | 1,493.8 | 1,258.2 |
| P9 | 1,200 | 21.9 | 1,605.3 | 1,046.2 |
| P10 | 1,200 | 50.1 | 878.7 | 651.0 |
| P11 | 1,200 | 16.1 | 2,396.4 | 2,063.7 |
| P12 | 1,000 | 17.8 | 1,641.2 | 1,590.8 |
| P13 | 900 | 18.8 | 1,268.7 | 893.6 |
| P14 | 600 | 17.5 | 625.1 | 708.5 |
| P15 | 1,500 | 28.6 | 2,047.3 | 1,571.3 |

| | | | | |
|---|---|---|---|---|
| P16 | 1,800 | 28.6 | 3,371.5 | ... |
| P17 | 1,500 | 28.7 | 2,523.8 | 2,018.5 |
| P18 | 1,000 | 27.5 | 1,128.5 | 1,099.6 |
| P19 | 1,200 | 27.5 | 1,825.4 | 1,968.9 |
| P20 | 800 | 27.6 | 759.4 | 835.1 |
| P21 | 1,800 | 29.8 | 3,221.2 | … |
| P22 | 1,800 | 33.8 | 2,697.1 | … |

Table 4.2 Settlements under the working load measured from signal matching of HSDT results and estimated from LSPT

| Pile ID | $K^{a,b}$ | $WL^c$ | LSPT $\delta^{d,e}$ | HSDT $\delta^d$ | $\Delta\delta^{d,f}$ | Percent[g] |
|---|---|---|---|---|---|---|
| P1 | 1541.4 | 2300 | 1.5 | 2.6 | -1.1 | -43 |
| P2 | 582.6 | 552 | 0.9 | 2.0 | -1.1 | -53 |
| P3 | 512.4 | 545 | 1.1 | 0.9 | 0.2 | 25 |
| P4 | 1477.3 | 612 | 0.4 | 0.6 | -0.2 | -33 |
| P5 | 428.3 | 3330 | 7.8 | 5.8 | 2.0 | 34 |
| P6 | 569.5 | 2400 | 4.2 | 4.6 | -0.3 | -08 |
| P7 | 1749.7 | 4425 | 2.5 | 2.4 | 0.2 | 07 |
| P8 | 1368.5 | 6725 | 4.9 | 4.5 | 0.4 | 09 |
| P9 | 1139.1 | 9829 | 8.6 | 6.1 | 2.5 | 41 |
| P10 | 711.5 | 7416 | 10.4 | 8.4 | 2.0 | 23 |
| P11 | 2240.1 | 2280 | 1.0 | 1.0 | 0.1 | 07 |
| P12 | 1728.4 | 1580 | 0.9 | 1.0 | 0.0 | -05 |
| P13 | 974.0 | 1278 | 1.3 | 1.0 | 0.3 | 30 |
| P14 | 773.7 | 557 | 0.7 | 0.9 | -0.2 | -19 |
| P15 | 1707.3 | 17670 | 10.3 | 8.6 | 1.7 | 20 |
| P16 | … | 25390 | … | 7.5 | … | … |
| P17 | 2191.2 | 15260 | 7.0 | 6.0 | 0.9 | 15 |
| P18 | 1196.9 | 7850 | 6.6 | 7.0 | -0.4 | -06 |
| P19 | 2137.5 | 10310 | 4.8 | 5.6 | -0.8 | -15 |

| | | | | | | |
|---|---|---|---|---|---|---|
| P20 | 910.7 | 5030 | 5.5 | 6.6 | -1.1 | -17 |
| P21 | … | 25390 | … | 7.9 | … | … |
| P22 | … | 26070 | … | 9.7 | … | … |

[a]reported in MN/m

[b]suggested static stiffness, calculated using Eq 4.1

[c]working load reported in kN

[d]settlement reported in mm

[e]calculated using Eq 4.2

[f]calculated using Eq 4.3

[g]calculated using Eq 4.4

### 4.1.2   Relationship between dynamic stiffness and value of EA/L

According to the PIT-W[TM] software user's manual, the initial dynamic stiffness relates to the elastic spring stiffness of a pile, and it can be compared to quantity EA/L of the pile. Lower values might indicate a defective or a lower shaft resistance while a higher value may relate to a bulge or higher shaft resistance. The static stiffness (K) determined from dynamic stiffness ($K_d$) and the value of EA/L estimated using an assumed E value of 25,000 MPa were plotted against each other as shown in Figure 4.4 and summarized in Table 4.3. A static stiffness value more than the value of EA/L is preferable since a pile having a higher stiffness could be considered as one with a comparatively high load-carrying capacity. On the other hand, a stiffness value lower than EA/L could be for a pile with a relatively lower load-carrying capacity. As shown in the Figure 4.4, dynamic stiffnesses of four piles (P2, P3, P7 and P8) are significantly less than the corresponding values of EA/L. It is observed that those piles have recorded small toe stiffnesses ($K_{toe}$) compared to their EA/L value (Table 4.3) and thus, it is evident that total stiffness of those piles are governed by the low toe stiffness. The load-settlement response at the toe, determined from the signal-matching technique of the CAPWAP[TM] software is used to calculate the toe stiffnes ($K_{toe}$).

It is interesting to see that suggested static stiffness and value of EA/L of rock-socketed bored piles show a positive correlation as shown in Figure 4.4. The visible trend is disturbed due to either a much higher $K_d$ value compared to EA/L or a much lower $K_d$

value compared to EA/L. However, a pile having a higher $K_d$ value than EA/L is always preferable as piles having lower $K_d$ values than EA/L (such as piles P2, P3, P7 and P8) have recorded relatively smaller toe stiffnesses. Therefore, direct comparison of K and/or $K_d$ with EA/L may be helpful to determine the comparable stiffness of the pile-soil-rock system and to determine doubtful rock-socketed, end-bearing bored piles with low skin friction and low toe stiffness.
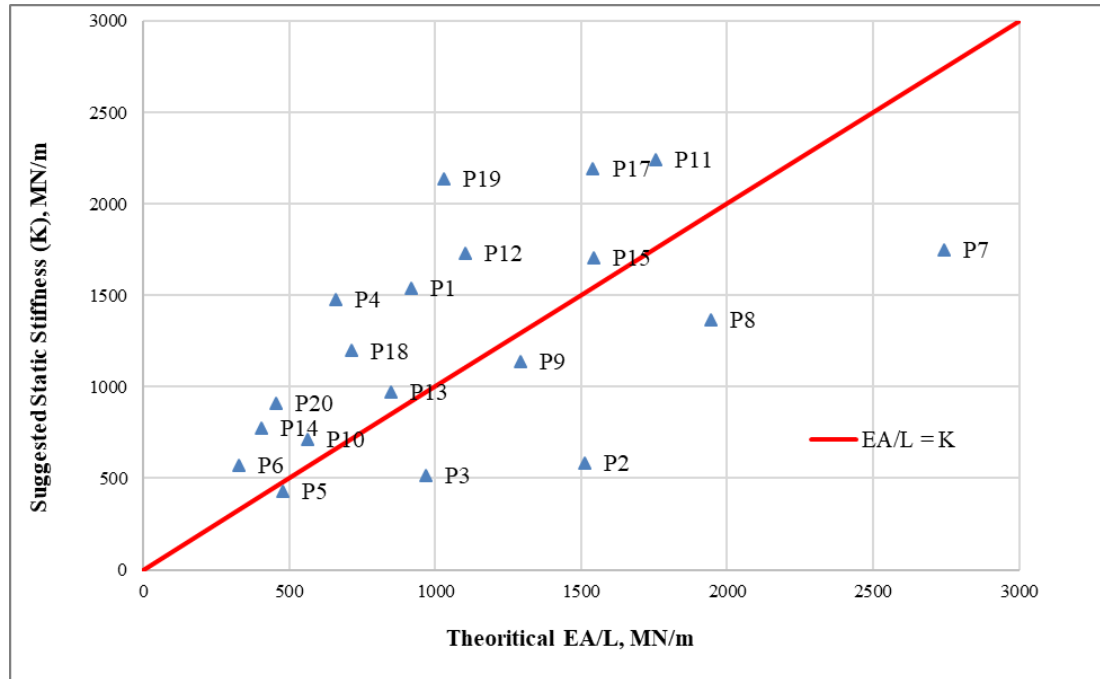


Figure 4.4 Comparison of suggested static stiffnesses and values of EA/L

Table 4.3 List of $K_d$, K, EA/L, $f_1$ and $K_{toe}$

| Pile ID | $K_d^a$ | $K^a$ | EA/L$^a$ | $f_1^b$ | $K_{toe}^a$ |
|---------|---------|-------|----------|---------|-------------|
| P1 | 1418.0 | 1541.4 | 917.5 | 85.0 | 2052.0 |
| P2 | 531.8 | 582.6 | 1514.0 | 68.0 | 145.0 |
| P3 | 467.0 | 512.4 | 968.3 | 80.0 | 0.0 |
| P4 | 1358.7 | 1477.3 | 661.4 | 80.0 | 1939.0 |
| P5 | 389.2 | 428.3 | 480.2 | 38.0 | 1460.0 |
| P6 | 519.7 | 569.5 | 327.2 | 50.0 | 750.0 |
| P7 | 1610.5 | 1749.7 | 2744.0 | 60.0 | 1512.0 |
| P8 | 1258.2 | 1368.5 | 1946.2 | 55.0 | 1174.0 |

| | | | | | |
|---|---|---|---|---|---|
| P9 | 1046.2 | 1139.1 | 1291.1 | 51.0 | 3786.0 |
| P10 | 651.0 | 711.5 | 564.4 | 33.0 | 4741.0 |
| P11 | 2063.7 | 2240.1 | 1755.1 | 70.0 | 4093.0 |
| P12 | 1590.8 | 1728.4 | 1103.1 | 70.0 | 10251.0 |
| P13 | 893.6 | 974.0 | 848.2 | 70.0 | 4353.0 |
| P14 | 708.5 | 773.7 | 403.5 | 70.0 | 3404.0 |
| P15 | 1571.3 | 1707.3 | 1542.6 | 100.0 | 19114.0 |
| P16 | … | 7.2 | 2221.3 | … | 5131.0 |
| P17 | 2018.5 | 2191.2 | 1541.5 | 65.0 | 14264.0 |
| P18 | 1099.6 | 1196.9 | 715.0 | 60.0 | 16212.0 |
| P19 | 1968.9 | 2137.5 | 1028.9 | 55.0 | 12535.0 |
| P20 | 835.1 | 910.7 | 454.6 | 58.0 | 3500.0 |
| P21 | … | … | 8104.1 | … | 19734.0 |
| P22 | … | … | 1882.7 | … | 29796.0 |

[a]reported in MN/m

[b]first resonant frequency reported in Hz

### 4.1.3   Base fixity of end bearing rock socketed piles

Base fixity of a pile is a major issue in the case of end bearing piles. In the case of a laterally unrestrained pile with infinitely rigid elastic base, the smallest frequency of resonance peak has a value of c/4L and in the event of a pile casted in to very soft material, the first resonant frequency occurs at a very low frequency [Davis, A.G. and Dunn, 1974]. If the position of first resonance frequency has a value equal to the half of frequency interval of the resonating total length of the pile, it is an indication of very rigid fixity [Chan, H.F.C., 1987]. Therefore, it is interesting to plot first resonant frequency of rock socketed end bearing piles and value of c/4L against pile length. The recorded wave velocity of concrete piles varies from 3,500 m/s to 4,500 m/s in Sri Lanka. Therefore, both upper and lower limit of velocity together with total pile length were used to calculate the value of c/4L. The comparison of first resonant frequency and c/4L is shown in Figure 4.5. The first resonant frequencies are listed in the Table 4.3.

As shown in Figure 4.5, the first resonant frequency mostly depends on pile length. When pile length increases first resonant frequency tends to reduce. However, some piles with the same length have recorded much different first resonant frequencies. Thus, there must be other factors that influence the first resonant frequency. The stiffness of pile-soil system has a greater influence on the location of first resonance frequency ($f_1$). Same-size piles that have different dynamic stiffness values may cause fluctuation of first resonant frequency.

Since most of tested piles have a large variation in diameter, length, and location it is difficult to compare one pile with another. However, piles P15 and P17 have the same in diameter and length. Pile P15 has recorded a much higher first resonant frequency than pile P17 as shown in Figure 4.5, while P17 has recorded a much higher value of dynamic stiffness than pile P15 even though it has recorded a small toe stiffness value compared to pile P15. Therefore, it is evident that toe stiffness has a greater influence on the first resonant frequency than combined effect of pile – soil stiffness.

Most of the first resonance frequencies are located on or above the lower value of c/4L (c = 3,500m/s). This may be an indication of the rigid base fixity of rock socketed end bearing piles. Only two cases were recorded much below the value of c/4L (c = 3,500 m/s). Although, pile P2 indicates a hard toe reflection as shown in Figure 4.6, it has recorded a very small dynamic stiffness compared to its value of EA/L (Table 4.3). Pile P3 indicates a relatively good dynamic stiffness. However, it indicates a soft-toe condition at the bottom as shown in Figure 4.7. Both of these piles have recorded small toe stiffnesses ($K_{toe}$), as indicated in Table 4.3, which is evident of weak bedrock, soft-toe condition, and/or defective pile section at toe. Thus, comparison of first resonant frequency with the value of c/4L against pile length will be helpful to determine doubtful rock socketed end bearing bored piles.
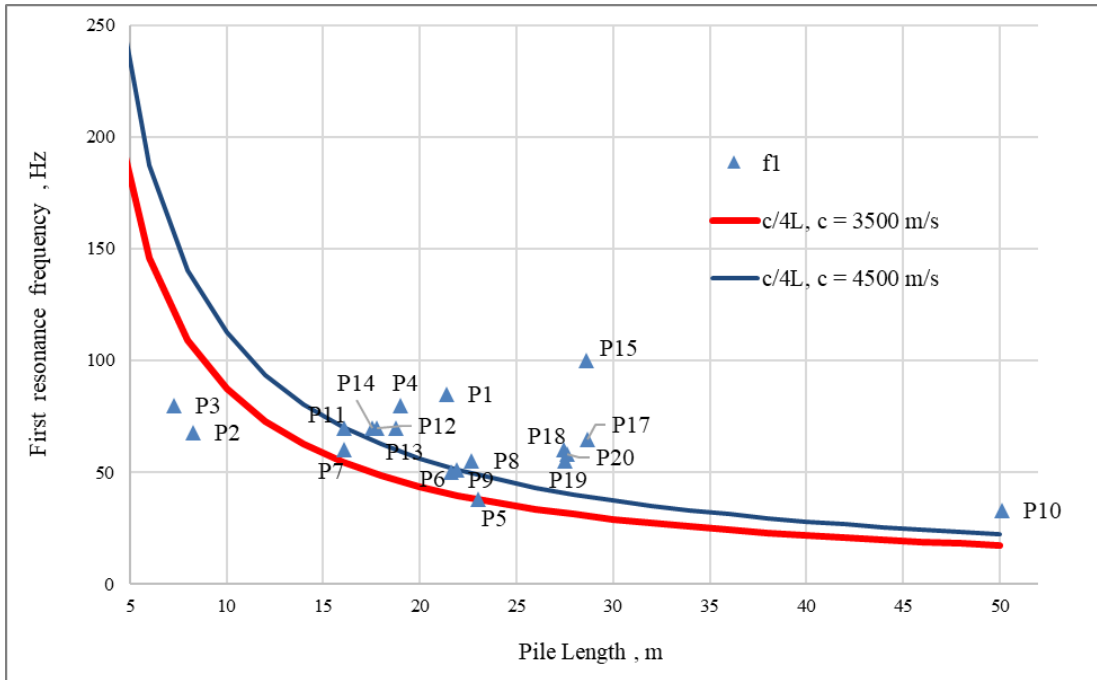
Figure 4.5 Comparison of first resonant frequency (f1) and value of c/4L
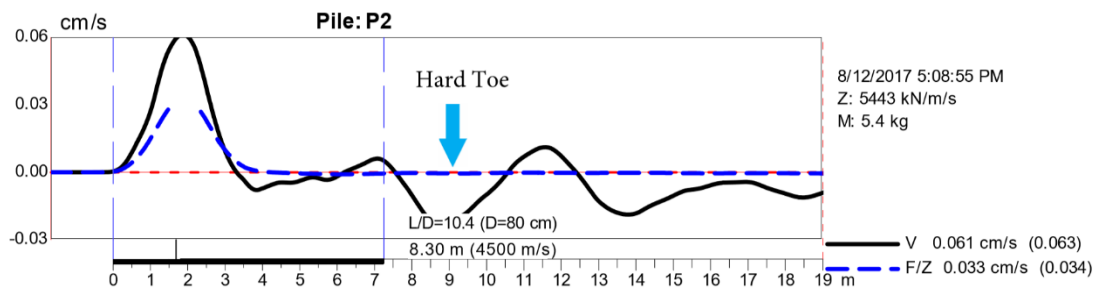


Figure 4.6 Time domain reflectogram of pile P2
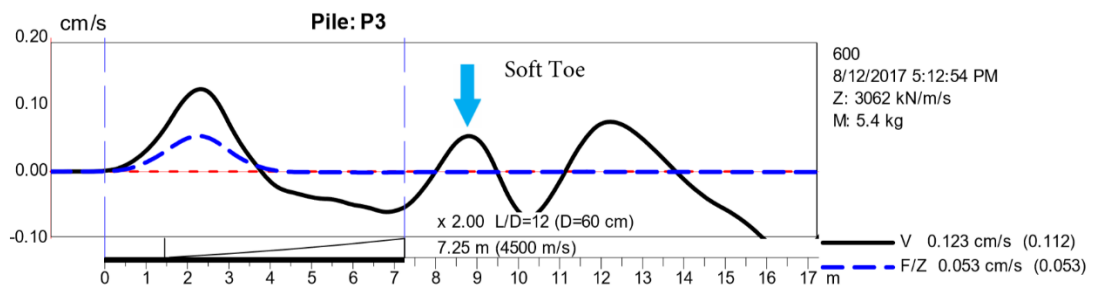


Figure 4.7 Time domain reflectogram of pile P3

### 4.1.4 Effective length

The total length of a defect free pile can be calculated using its regular peak pattern in the high frequency range, as indicated in Eq 2.7. A regular peak pattern of 124.2 Hz was observed in the pile P7, indicating the total length of 16.1m as shown in Figure 4.8. The frequency interval pattern can be used to detect the smaller anomaly and length of the pile as shown Figure 4.9 and 4.10 respectively for piles P9 and P23. At the depth of 6.9m, a small bulging is observed in the pile P9 and a necking was visible in the pile P23. The pile lengths can also be identified as 21,9m and 13.5m respectively as observed in Figures 4.9 and 4.10.

The length up to the damage is measured on the mobility plot if the pile is broken [Davis, A.G. and Dunn., 1974] and if bulging is larger, its position can be estimated but not the overall length as observed in the pile P10 (Figure 4.11). In that case, the depth to the major bulging was recorded as 7.8m. But, in such situations, it is arguable which section of the pile provides the base condition. It is doubtful whether a peak pattern with a regular frequency interval will ever develop in the piles with an irregular shape or multiple defects. In such cases, complex peak patterns may be resulted and it will be almost impossible to determine the effective length. The peak pattern with a regular frequency interval has not been developed in the pile P17 due to irregular shape of the pile as shown in Figure 4.2.
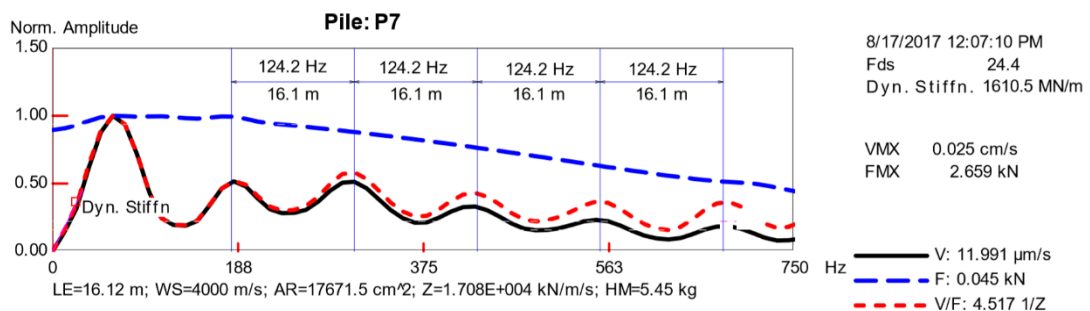


Figure 4.8 Mobility spectrum of pile P7
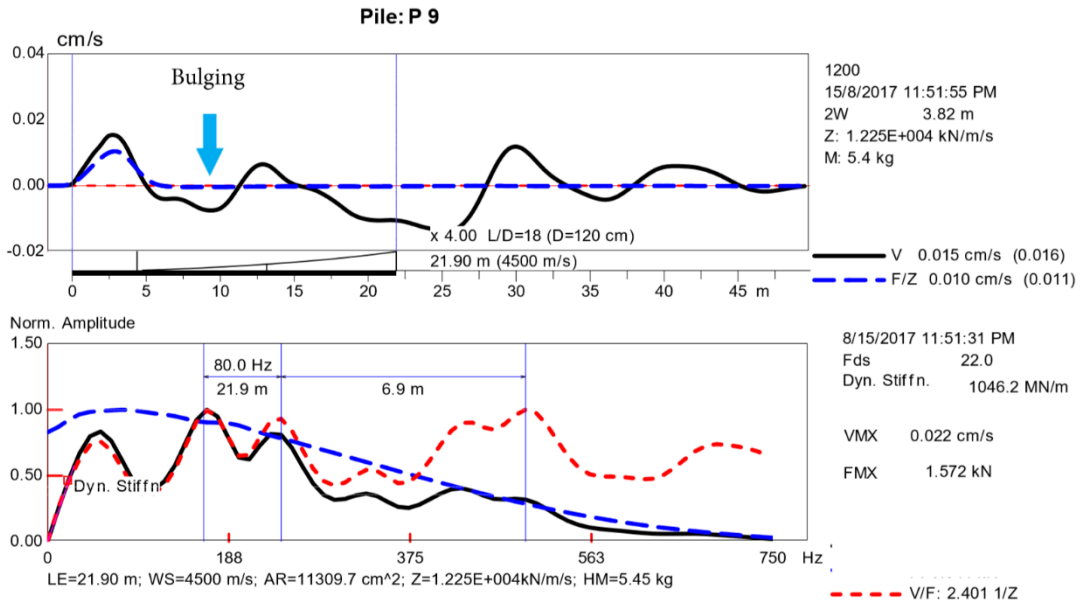
Figure 4.9 Time domain reflectogram and mobility spectrum of pile P9
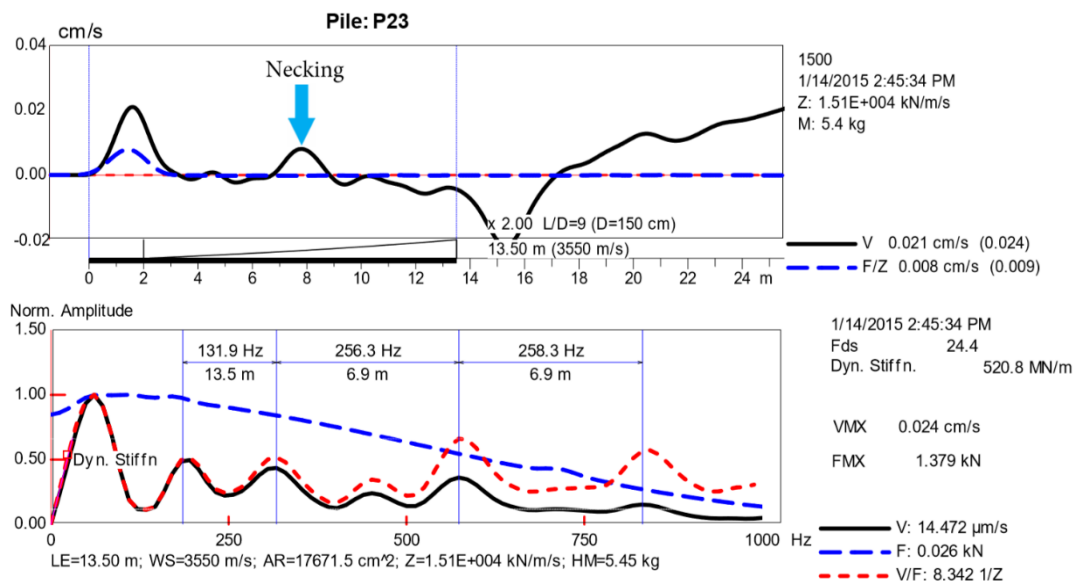


Figure 4.10  Time domain reflectogram and mobility spectrum of pile P23
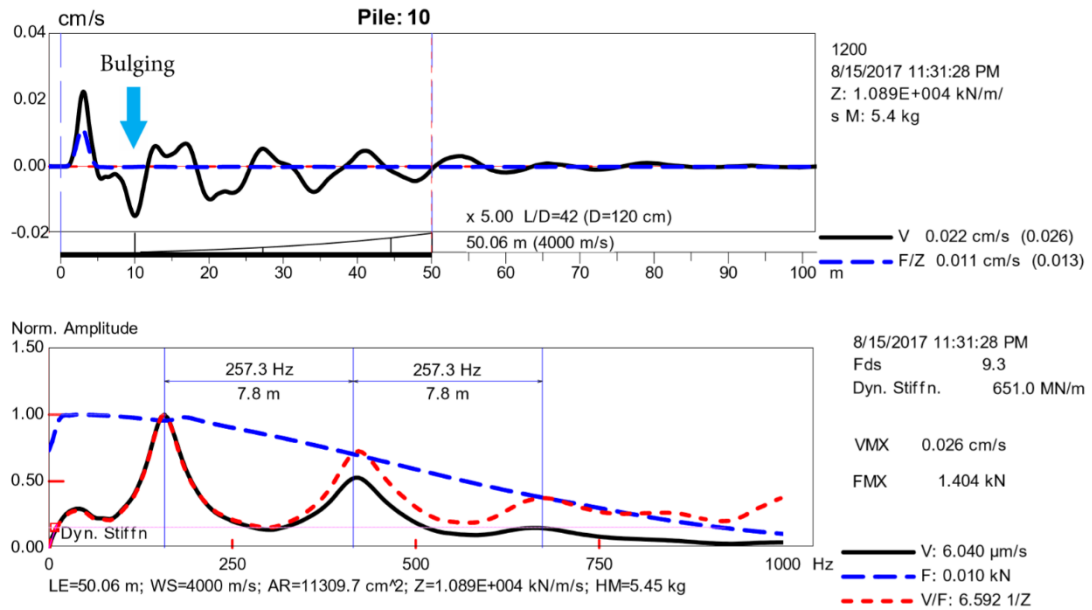
Figure 4.11 Time domain reflectogram and mobility spectrum of pile P10

## 4.2 Developing a methodology to estimate the allowable bearing capacity of bored piles

### 4.2.1 Shaft shortening due to the pile top load in the linear zone of load-settlement graph (pile set 1)

The pile toe settlement is subtracted from the pile top displacement to estimate the shaft elastic shortening. The elastic shortening was plotted against the PL/AE value as visible in Figure 4.12. A value of 0.98 received for the coefficient of determination ($R^2$) as shown in Figure 4.12. As observed in this result, there is a little influence from socket length, pile length, pile diameter and location towards the fraction of elastic shortening, the fixity provided at the toe level could be the reason. The elastic shortening can be taken as 062PL/AE based on the graph.
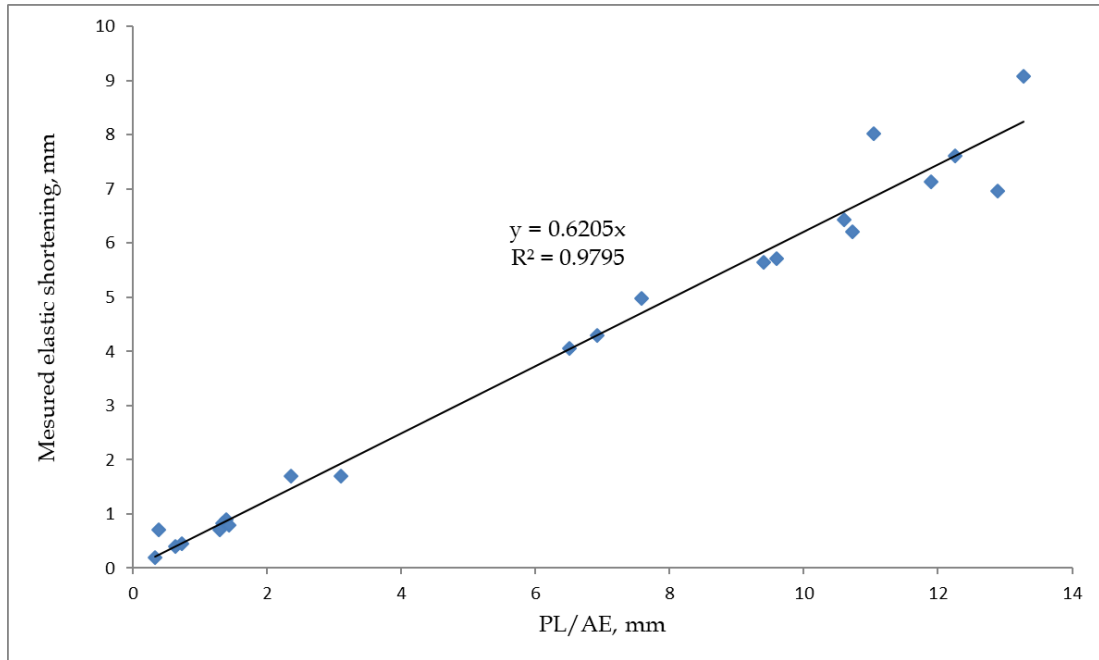
Figure 4.12 Observed elastic shortening vs. PL/AE of linear region

## 4.2.2 Shaft shortening due to the pile top load in the non-linear zone of load-settlement graph (pile set 2)

Generally, mobilized loads of high strain dynamic load testing reach the no-linear zone of load settlement graph. But pile doesn't reach the non-linear region with small settlements. Thus, this scenario can be identified as a limitation of high strain dynamic load testing. Therefore, it is always recommended to use piles with higher settlements to estimate elastic shortening in the non-linear region. But, when observe the load-settlement curves of pile set 2, some piles have clearly developed a second region in the graphs. Based on those results, elastic shortening was plotted against the PL/AE value as shown in Figure 4.13. The coefficient of determination of 0.92 is observed in the graph. Therefore, actual shat shortening can be taken as 0.64 PL/AE.
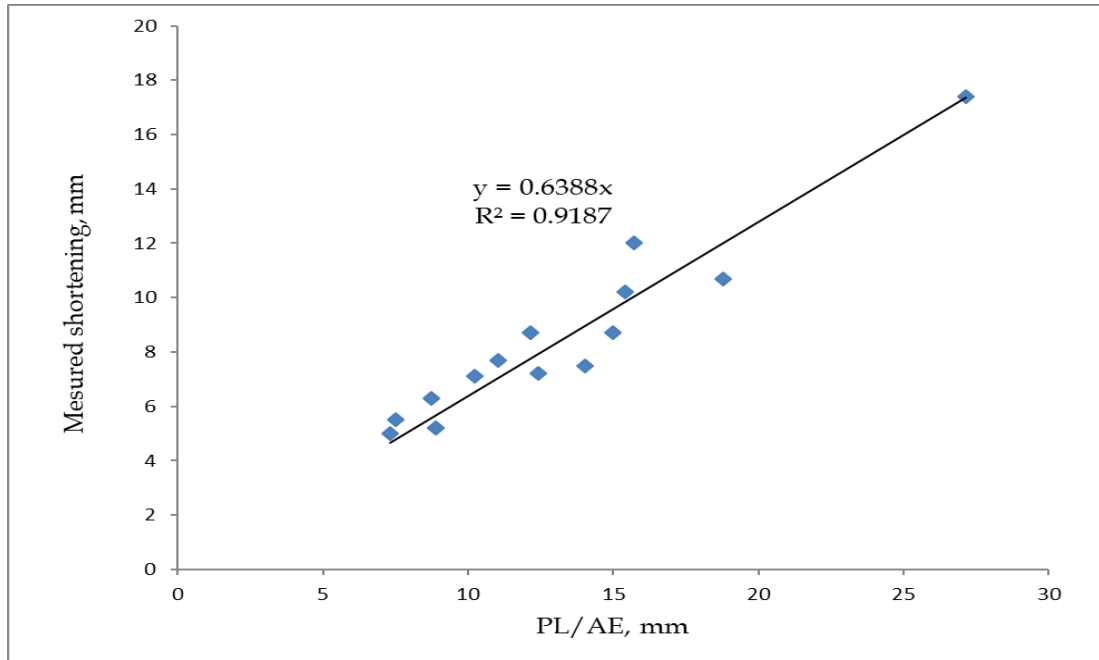
Figure 4.13 Observed elastic shortening vs. PL/AE of non- linear region

### 4.2.3 Pile toe displacement under a Load

The pile toe movement criterion was developed based on the studies of toe movements in the linear and non-linear zones of load settlement graphs. Generally, small pile toe displacement is visible in rock socketed piles and shaft shortening of piles has a greater influence towards the total settlement.

The pile toe movement can be taken as a function of pile toe stiffness and pile toe load. Therefore, stiffness of pile toe and load of pile toe are estimated. The pile toe load shall be successfully correlated to pile top load as shown in Figure 4.14 and 4.15 for both regions. The pile toe load in linear zone can be taken as 0.51 times the pile top load whereas, 0.58 times the pile top load in the non-linear zone. But it recommended to derive site-based relationships to estimate the pile toe load. Finally, both criterions are calculated using Eq. 4.5 and Eq. 4.6
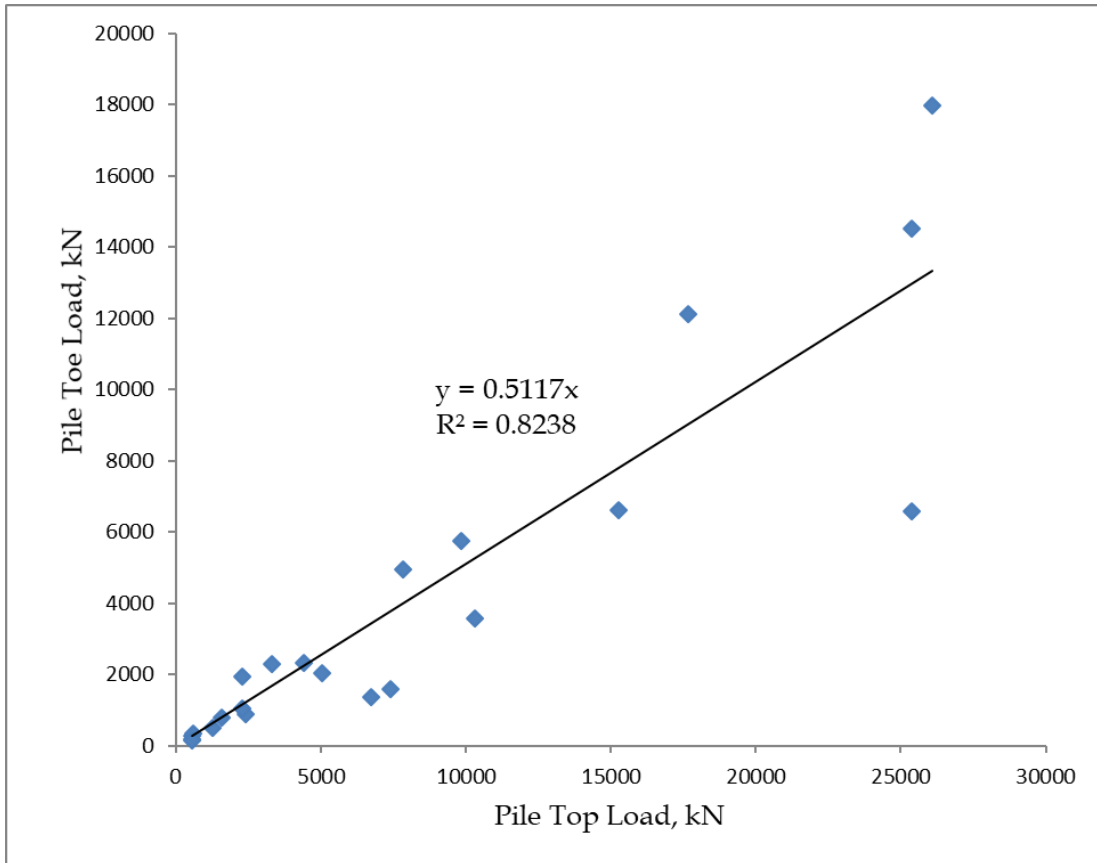
Figure 4.14 Pile toe load vs pile top load in linear zone of load settlement graph

For linear region of load-displacement graph,

$$\Delta_{linear} = 0.62 \frac{P_{top}L}{AE} + 0.51 \frac{P_{top}}{K_{toe}} \dots\dots\dots\dots\dots\dots\dots\dots\dots\dots\dots\dots\dots\dots\dots (4.5)$$

For non-linear zone of load-settlement graph,

$$\Delta_{non-linear} = 0.64 \frac{P_{top}L}{AE} + 0.58 \frac{P_{top}}{K_{toe}} \dots\dots\dots\dots\dots\dots\dots\dots\dots\dots\dots\dots\dots (4.6)$$

A correlation can be used in the initial linear zone of the load-settlement curve to estimate pile toe stiffness as shown in Eq. 4.7.

$$P_{top} = K \times \Delta_{linear} \dots\dots\dots\dots\dots\dots\dots\dots\dots\dots\dots\dots\dots\dots\dots\dots\dots (4.7)$$

$K$ = static stiffness
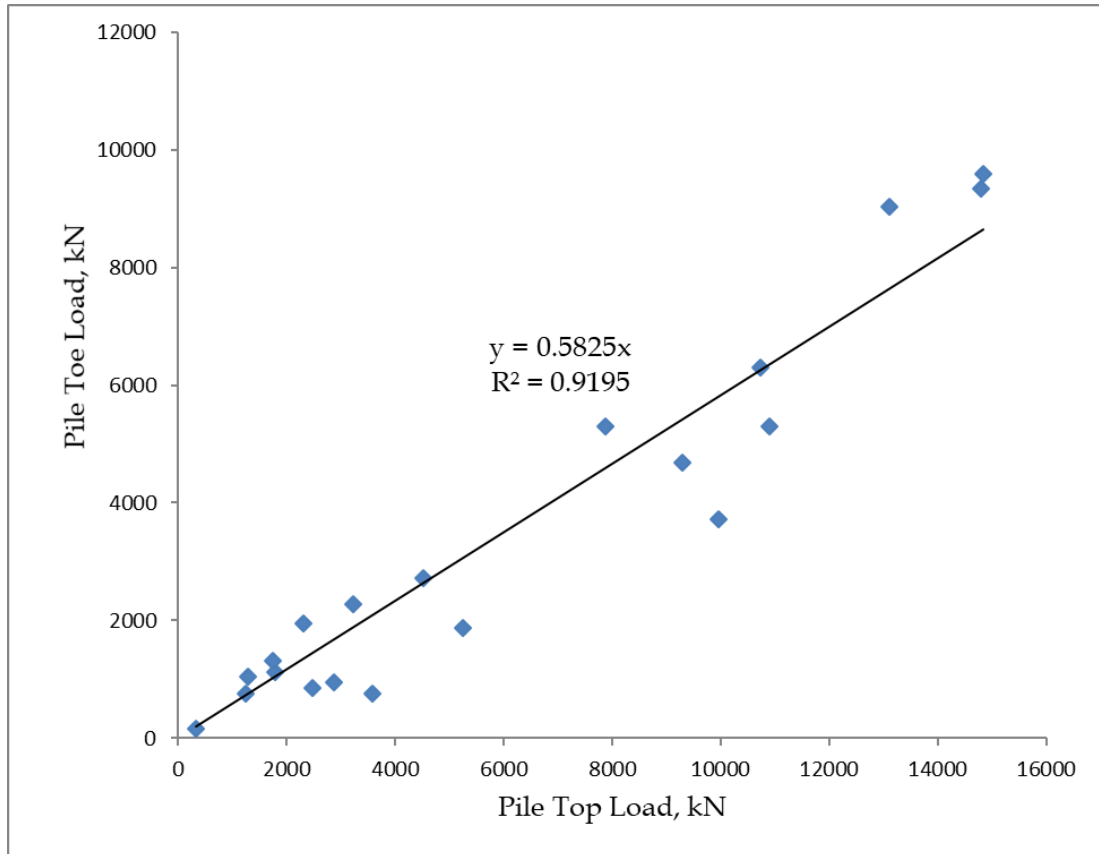
Figure 4.15 Pile toe load vs pile top load in non-linear zone of load settlement graph

Static stiffness can be calculated using Eq. 4.1.

$$\text{ie, } K = 1.082 \times K_d + 7.151 \dots\dots\dots\dots\dots\dots\dots\dots\dots\dots\dots\dots\dots\dots\dots (4.1)$$

$K_d$ = dynamic stiffness

From the Eq. 4.6 and 4.7, following equation can be formulated,

$$P_{top} = K \times \left[ 0.62 \frac{P_{top}L}{AE} + 0.51 \frac{P_{top}}{K_{toe}} \right] \dots\dots\dots\dots\dots\dots\dots\dots\dots\dots\dots (4.8)$$

Following equation can be written from Eq. 4.8,

$$K_{toe} = \frac{0.51}{\left[ \frac{1}{K} - 0.62 \frac{L}{AE} \right]} \dots\dots\dots\dots\dots\dots\dots\dots\dots\dots\dots\dots\dots\dots (4.9)$$

In order to satisfy the above equation,

$$\left[\frac{1}{K} - 0.62\frac{L}{AE}\right] > 0$$

i.e,

$$K < \frac{AE}{0.62L}$$

The K value reaches to infinity when K is equal to AE/0.62L. Therefore, K value should be limited in Eq. 4.8 to AE/0.62L.

### 4.2.4 Allowable carrying capacity estimation

The vertical allowable bearing capacity can be estimated using following steps. The derived equations in the previous chapters are used.

**Step 1:**

A smooth surface should be prepared for the sensor attachment and hammer hit. Conduct the instrumented low strain pile integrity testing accurately. The measurement should be analyzed and interpreted. Estimate the dynamic stiffness from frequency domain analysis.

**Step 2:**

Calculate the static stiffness (K) from the Eq. 4.1 and maximum value is AE/0.62L.

**Step 3:**

Calculate the toe stiffness from Eq. 4.9.

**Step 4:**

Calculate structural capacity from Eq 4.10.

$$\text{Structural capacity} = 0.25 \times f_{cu} \times A \dots\dots\dots\dots\dots\dots\dots\dots\dots\dots\dots\dots\dots\dots\dots\dots\dots\dots \;\; (4.10)$$

$f_{cu}$ = concrete strength

A = pile cross sectional area

**Step 5:**

Use the structural capacity estimated from Eq. 4.10 in the Eq. 4.6 and calculate the relevant displacement. With a vertical loading it is assumed that pile always reaches to the non-linear region as a conservative approach. If the settlement is less than settlement limit (CIDA guild lines – 12mm) specified at the site, the structural capacity shall be used as the allowable bearing capacity. But, if the displacement is greater than the settlement limit, $P_{top}$ is back calculated using allowable limit and consider this $P_{top}$ as the allowable bearing capacity.

The estimated allowable carrying capacities are listed in Table 4.5. As seen in the results, most of piles exceed the allowable settlement limit when loaded to the structural capacity. Therefore, allowable capacities of those piles are limited to the allowable settlement limit of 12mm. However, different allowable settlement limits shall be adopted based on the requirement.

High strain dynamic load testing results are compared with the proposed methodology to verify the accuracy. The mobilized settlements in the high strain dynamic load tests are applied in the proposed settlement criterion and pile top load is back calculated. This pile top load is considered as the predicted mobilized load. After that, this mobilized pile load is compared with the actual mobilized load from load testing results. as shown in Figure 4.16. The results are shown in Table 4.6. As shown in the graph a strong relationship can be observed with coefficient of determination of 0.92. And proposed methodology slightly under predicts the actual mobilized load. Thus, it is verified that suggested methodology provides conservative and accurate results.
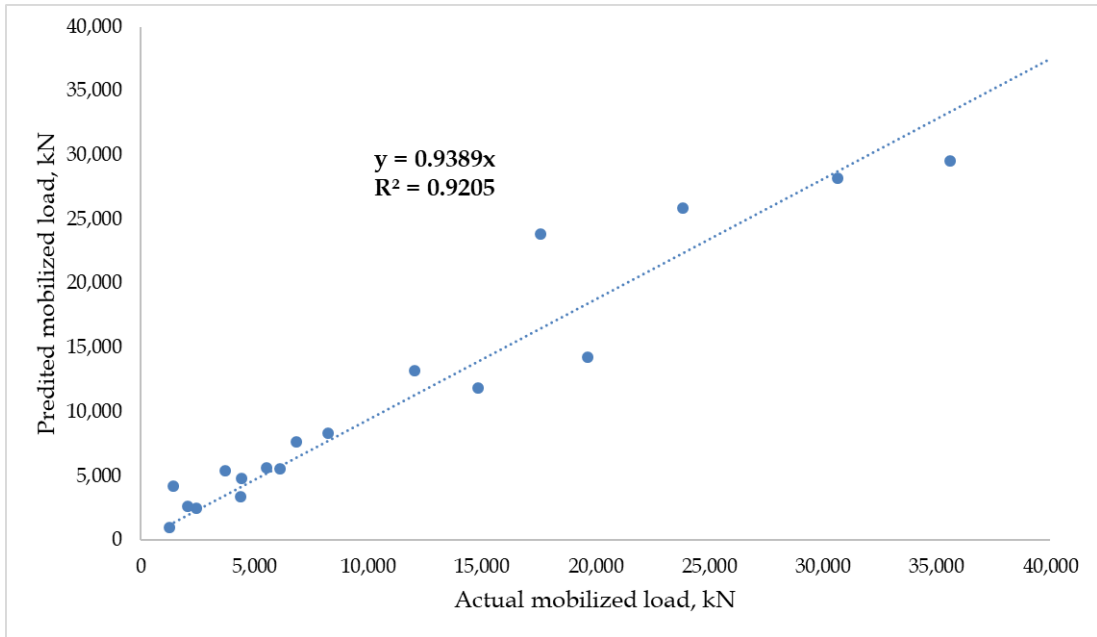
Figure 4.16 Forecasted pile top load vs true mobilized pile load

Table 4.4 HSDT Results

| | Linear Region – Set 1 | | | | | | | Non-linear region – Set 2 | | | | | | |
|---|---|---|---|---|---|---|---|---|---|---|---|---|---|---|---|
| Pile No | Top Load[a] | Toe Load[a] | $P_{toe}/P$ | Top $\delta$[b] | Toe $\delta$[b] | $\Delta\ \delta$[b] | PL/AE[b] | Pile No | Top Load[a] | Toe Load[a] | $P_{toe}/P$ | Top $\delta$[b] | Toe $\delta$[b] | $\Delta\ \delta$[b] | PL/AE[b] |
| P1 | 3330 | 2292 | 0.69 | 5.66 | 1.60 | 4.06 | 6.51 | L1 | 9958 | 3727 | 0.37 | 12.5 | 8.8 | - | - |
| P2 | 2400 | 877 | 0.37 | 5.49 | 1.20 | 4.29 | 6.93 | L2 | 14795 | 9346 | 0.63 | 12.7 | 5.6 | 7.1 | 10.25 |
| P3 | 4425 | 2324 | 0.53 | 2.40 | 1.50 | 0.90 | 1.39 | L3 | 14846 | 9585 | 0.65 | 13.2 | 5.5 | 7.7 | 11.06 |
| P4 | 6725 | 1365 | 0.20 | 5.50 | 3.80 | 1.70 | 3.10 | L4 | 1253 | 762 | 0.61 | 19.8 | 14.3 | 5.5 | 7.52 |
| P5 | 9829 | 5747 | 0.58 | 6.48 | 1.50 | 4.98 | 7.58 | L5 | 3578 | 759 | 0.21 | 8.7 | 3.5 | 5.2 | 8.88 |
| P6 | 7416 | 1595 | 0.22 | 7.27 | 0.30 | 6.97 | 12.89 | L6 | 7883 | 5302 | 0.67 | 8.9 | 4.9 | - | - |
| P7 | 2280 | 1054 | 0.46 | 0.90 | 0.20 | 0.70 | 0.39 | L7 | 4517 | 2711 | 0.60 | 14.6 | 4.4 | 10.2 | 15.40 |
| P8 | 1580 | 778 | 0.49 | 0.90 | 0.07 | 0.83 | 1.34 | L8 | 335 | 156 | 0.47 | 10.2 | 9.6 | - | - |
| P9 | 1278 | 492 | 0.38 | 0.90 | 0.10 | 0.80 | 1.43 | L9 | 10732 | 6308 | 0.59 | 19.6 | 2.2 | 17.4 | 27.16 |
| P10 | 557 | 140 | 0.25 | 0.70 | 0.00 | 0.70 | 1.30 | L10 | 3233 | 2279 | 0.70 | 10.3 | 2.8 | 7.5 | 14.04 |
| P11 | 17670 | 12108 | 0.69 | 8.63 | 0.60 | 8.03 | 11.04 | L11 | 1797 | 1133 | 0.63 | 7.9 | 5.7 | - | - |
| P12 | 25390 | 6583.5 | 0.26 | 8.82 | 1.21 | 7.61 | 12.25 | L12 | 5250 | 1875 | 0.36 | 8.5 | 1.3 | 7.2 | 12.41 |
| P13 | 15260 | 6620 | 0.43 | 6.05 | 0.40 | 5.65 | 9.40 | L13 | 1284 | 1054 | 0.82 | 15.4 | 9.1 | 6.3 | 8.73 |
| P14 | 7850 | 4944 | 0.63 | 7.03 | 0.60 | 6.43 | 10.60 | L14 | 13103 | 9032 | 0.69 | 6 | 1.5 | - | - |
| P15 | 10310 | 3590 | 0.35 | 5.99 | 0.28 | 5.71 | 9.59 | L15 | 10900 | 5307 | 0.49 | 9.4 | 0.7 | 8.7 | 14.99 |
| P16 | 5030 | 2042 | 0.41 | 6.75 | 0.54 | 6.21 | 10.73 | L16 | 9286 | 4676 | 0.50 | 14.1 | 3.4 | 10.7 | 18.80 |
| P17 | 25390 | 14530 | 0.57 | 7.85 | 0.71 | 7.14 | 11.89 | L17 | 2868 | 949 | 0.33 | 8 | 2.8 | 5.2 | 8.89 |
| P18 | 26070 | 17984 | 0.69 | 9.75 | 0.66 | 9.09 | 13.28 | L18 | 1739 | 1308 | 0.75 | 18.2 | 9.5 | 8.7 | 12.15 |

| | | | | | | | | | | | | | | | |
|---|---|---|---|---|---|---|---|---|---|---|---|---|---|---|---|
| P19 | 2300 | 1946 | 0.85 | 2.70 | 1.00 | 1.70 | 2.36 | L19 | 2305 | 1954 | 0.85 | 32.3 | 20.3 | 12 | 15.70 |
| P20 | 552 | 269 | 0.49 | 2.09 | 1.89 | 0.20 | 0.33 | L20 | 2486 | 847 | 0.34 | 12.4 | 7.4 | 5 | 7.32 |
| P21 | 545 | 184 | 0.34 | 0.80 | 0.40 | 0.40 | 0.64 | | | | | | | | |
| P22 | 612 | 337 | 0.55 | 0.65 | 0.20 | 0.45 | 0.73 | | | | | | | | |

[a] in kN in mm

[b] in mm

[c] in MN/m ,

[d] in mm$^2$

Table 4.5  Allowable carrying capacity estimation

| Pile No | $PDA_K$[c] | $PIT_{Kd}$[c] | $D$[b] | $A$[d] | $AE/L$[c] | $K$[c] | $K_{max}$[c] | $K_{toe}$[c] | $f_{cu}$[c] | $P_{structural}$[a] | $\delta_{structural}$[b] | $\delta_{allowable}$[b] | $P_{allowable}$[a] |
|---|---|---|---|---|---|---|---|---|---|---|---|---|---|
| P1 | 881 | 1418 | 1000 | 785398 | 918 | - | - | - | 25 | 19,635 | 14 | 12 | 17,204 |
| P2 | 273.1 | 531.8 | 800 | 502655 | 1478 | 583 | 583 | 362 | 25 | 12,566 | 25 | 12 | 6,065 |
| P3 | 640.2 | 467 | 600 | 282743 | 968 | 512 | 512 | 358 | 25 | 7,069 | 16 | 12 | 5,398 |
| P4 | 982.9 | 1358.7 | 880 | 608212 | 661 | 1477 | 1067 | infinity | 25 | 15,205 | 15 | 12 | 12,401 |
| P5 | 573.4 | 389.2 | 750 | 441786 | 480 | 428 | 428 | 450 | 25 | 11,045 | 28 | 12 | 4,657 |
| P6 | 526.3 | 519.7 | 600 | 282743 | 327 | 569 | 528 | infinity | 25 | 7,069 | 14 | 12 | 6,136 |
| P7 | 1870.7 | 1610.5 | 1500 | 1767146 | 2744 | 1750 | 1750 | 1360 | 25 | 44,179 | 28 | 12 | 18,605 |
| P8 | 1493.8 | 1258.2 | 1500 | 1767146 | 1946 | 1369 | 1369 | 1140 | 25 | 44,179 | 36 | 12 | 14,636 |
| P9 | 1605.3 | 1046.2 | 1200 | 1130973 | 1291 | 1139 | 1139 | 1182 | 25 | 28,274 | 27 | 12 | 12,378 |
| P10 | 878.7 | 651 | 1200 | 1130973 | 564 | 712 | 712 | 1532 | 25 | 28,274 | 42 | 12 | 8,002 |
| P11 | 2396.4 | 2063.7 | 1200 | 1130973 | 1755 | 2240 | 2240 | 5045 | 25 | 28,274 | 13 | 12 | 25,229 |

| P12 | 1641.2 | 1590.8 | 1000 | 785398 | 1103 | 1728 | 1728 | 28464 | 25 | 19,635 | 12 | 12 | 20,005 |
|-----|--------|--------|------|---------|------|------|------|----------|----|--------|----|----|--------|
| P13 | 1268.7 | 893.6 | 900 | 636173 | 848 | 974 | 974 | 1589 | 25 | 15,904 | 18 | 12 | 10,841 |
| P14 | 625.1 | 708.5 | 600 | 282743 | 403 | 774 | 651 | infinity | 25 | 7,069 | 11 | 12 | 7,565 |
| P15 | 2047.3 | 1571.3 | 1500 | 1767146 | 1543 | 1707 | 1707 | 2557 | 25 | 44,179 | 28 | 12 | 18,931 |
| P16 | 3371.5 | - | 1800 | 2544690 | 2221 | - | - | - | 25 | 63,617 | - | 12 | - |
| P17 | 2523.8 | 2018.5 | 1500 | 1767146 | 1541 | 2191 | 2191 | 8677 | 25 | 44,179 | 21 | 12 | 25,014 |
| P18 | 1128.5 | 1099.6 | 1000 | 785398 | 715 | 1197 | 1153 | infinity | 25 | 19,635 | 18 | 12 | 13,407 |
| P19 | 1825.4 | 1968.9 | 1200 | 1130973 | 1029 | 2138 | 1660 | infinity | 25 | 28,274 | 18 | 12 | 19,292 |
| P20 | 759.42 | 835.1 | 800 | 502655 | 455 | 911 | 733 | infinity | 25 | 12,566 | 18 | 12 | 8,525 |

Table 4.6  Pile top load calculation from proposed methodology with the actual mobilized settlement

| Pile No | $\delta_{mobilized}$[b] | $P_{mobilize}$[a] | $P_{calculated}$[a] |
|---------|-----------|-----------|-----------|
| P1 | 8.6 | 3,741 | - |
| P2 | 8.6 | 1,451 | 4,229 |
| P3 | 2.3 | 1,267 | 1,009 |
| P4 | 2.6 | 2,074 | 2,687 |
| P5 | 14.7 | 6,122 | 5,609 |
| P6 | 10.6 | 3,707 | 5,420 |
| P7 | 5.5 | 8,262 | 8,337 |
| P8 | 6.4 | 6,833 | 7,642 |
| P9 | 14.1 | 19,658 | 14,294 |
| P10 | 18.0 | 14,833 | 11,900 |
| P11 | 2.7 | 5,525 | 5,630 |
| P12 | 2.9 | 4,434 | 4,829 |
| P13 | 3.8 | 4,395 | 3,394 |
| P14 | 4.0 | 2,442 | 2,522 |
| P15 | 19.0 | 35,588 | 29,609 |
| P16 | 18.9 | 41,793 | |
| P17 | 13.6 | 30,629 | 28,214 |
| P18 | 21.4 | 17,597 | 23,909 |
| P19 | 16.1 | 23,859 | 25,883 |
| P20 | 18.6 | 12,037 | 13,213 |

# CHAPTER 5.    DISCUSSION

Reliable results can only be obtained from perfect measurements at the pile top. Thus, it may be necessary to cut some pile section to receive the good concrete and small zones should be prepared to provide a smooth surface for attachment of the motion sensor and for the impact. Mobility is affected by the impedance and the relative magnitude of the velocity and the force applied during the testing. The irregular shape of cast in situ piles may yield inconsistent values of mobility. In such cases, attention is usually paid for more important parameters such as dynamic stiffness and effective length of a pile. Rausche et al, 1992 stated that if the mobility is linear in the range of 0 – 100 Hz, the dynamic stiffness is valid. However, it was observed through the test results, even if the mobility is linear in the region of 0 to 30Hz, the dynamic stiffness value yields fairly accurate results for rock socketed end bearing piles.

There are impact hammers with different weights and sizes. Small hammers produce low energy while large hammers produce high energy. Due to the higher impact energy induced by large hammers, the stress waves are not quickly attenuated and can penetrate to deeper level of the pile. Large hammers produce wider impact pulse than small hammers. However, defects near the pile top may be masked by the input pulse of large hammer. Different hammers will result in different excitation signals and frequency content and the lower frequency signals propagate further. However, their reflections are less clearly defined and thus, become more difficult to read than higher frequency signals [Rausche et al, 2002].

It is often difficult to judge defects solely from the frequency analysis or the time-domain analysis. Frequency-domain analysis reveals more information than conventional time- domain analysis. However, the transient response method (frequency domain analysis) might not be able to detect the defects near the pile toe as reflections from the pile toe may not be differentiated from the toe signal. In the time-domain analysis it might be difficult to detect the defects near the pile top as input pulse may mask the reflections from defects near the pile top. However, the transient response method clearly reveals the impedance changes near the pile top.

# CHAPTER 6.    CONCLUSION

It was verified that the dynamic stiffness at low frequencies is related to the initial slope of the load – displacement graph for an end bearing pile. Therefore, the TDR method can be used to determine the load – settlement behavior of a pile in the zone of the expected working load. However, it is doubtful that the dynamic stiffness is meaningful when the peak pattern indicates depth to the major anomaly instead of total pile length. In such cases, an advanced method would be needed to determine the static stiffness of the piles or direct use of pile load tests.

From the analysis of the case studies, it is suggested that the static stiffness and/or dynamic stiffness can be compared with value of EA/L to determine doubtful rock-rocketed, end-bearing, bored piles, and the first resonance frequency of pile-soil-rock system is an indication of the base fixity of rock socketed end bearing piles. Furthermore, the first resonant frequency is influenced by pile length, toe stiffness, and stiffness of pile-soil-rock system. Moreover, the first resonant frequency and the value of c/4L can also be used to identify doubtful rock- rocketed, end-bearing, bored piles.

The combined test results of transient dynamic method and pulse-echo method will give a more comprehensive details of the pile than either test alone. In some cases, it may not be possible to determine all the parameters as outlined in this research. Thus, attention should be paid to the more important parameters such as the effective length of a pile and the dynamic stiffness.

In the section 4.2, it was verified that the allowable bearing capacity of rock socketed bored piles shall successfully be estimated from the instrumented low strain pile integrity testing results. For the defective piles, advanced load testing method such as high strain dynamic load testing or static load testing shall be used to estimate the allowable carrying capacity.

# CHAPTER 7.    REFERENCES

[1] T. H. Kodithuwakku, H. S. Thilakasiri, and A. Rathnayaka, "Case Studies: Use of Low Strain Transient Dynamic Response Method for Rock Socketed End Bearing Bored Piles," in *10th International Conference on Stress Wave Theory and Testing Methods for Deep Foundations*, ed. P. Bullock, G. Verbeek, S. Paikowsky, and D. Tara (West Conshohocken, PA: ASTM International, 2019), 205-222. https://doi.org/10.1520/STP161120170194

[2] T. H. Kodithuwakku and H. S. Thilakasiri, "Allowable carrying capacity estimation of bored piles using low strain pile integrity test," in *17th European Conference on Soil Mechanics and Geotechnical Engineering*, Iceland, 2019.

https://www.issmge.org/uploads/publications/51/75/0992-ecsmge-2019_Kodithuwakku.pdf

[3] Cooray, P.G., *The Geology of Sri Lanka (Ceylon)*, National Museums of Sri Lanka Publication, Colombo 07,1984, p. 77

[4] Thilakasiri H.S., "Evaluation of the Design and Construction Practices of Pile Foundation in Sri Lanka," *ICTAD Quality Journal*, Vol. 4, November 2006.

[5] Rausche, F., Ren - Kung, S. and Likins, G., "A comparison of pulse echo and transient response pile integrity test methods," presented at the *seventieth Annual Transportation Research Board Meeting*, Washington, D.C. 1991.

[6] Rausche, F., "Non – Destructive Evaluation of Deep Foundations," presented at the *fifth international conference on case histories in geotechnical engineering*, New York, NY, 1-9, 2004.

[7] Liang, L. and Beim, J., "Effect of soil resistance on low strain mobility response of piles using impulse transient response method," presented at the *eighth international conference on the application of stress wave theory to piles*, Lisbon, Portugal; 435-441, 2008. http://web.archive.org/web/20180421115235/https://www.grlengineers.com/wp-content/uploads/2008/09/CH-7-066-001.pdf (accessed 21 Apr. 2018)

[8] Davis, A.G. and Dunn., "From theory to field experience with the non-destructive vibration testing of piles," *Proc. Instn. Civ. Engrs. Part 2*, 57, December, 1974.

[9] Chan, H.F.C., "Non-destructive testing of concrete piles using the sonic echo and transient shock method," doctoral thesis, University of Edinburgh, 1987. http://web.archive.org/web/20180421114624/https://www.era.lib.ed.ac.uk/handle/1842/13349 (accessed 21 Apr. 2018)

[10] Thilakasiri, H.S., *Construction and Testing of Piles*, Sarasavi Publishers, Sri Lanka, 2009, pp. 229-230.

[11] Pile Dynamic Inc. (2009). PIT-W software for pile integrity tester: Instruction manual. Cleveland, Ohio, USA, MA: Author

[12] ASTM D 5882 – 07, *Standard Test Method for Low Strain Impact Integrity Testing of Deep Foundations*, ASTM International, West Conshohocken, PA, www.astm.org.

[13] ASTM D 4945 – 17, *Standard Test Method for High Strain Dynamic Testing of Deep Foundations*, ASTM International, West Conshohocken, PA, www.astm.org

[14] Rausche, F., Likins, G.E. and Ren-Kung, S., "Pile integrity testing and analysis," presented at *the fourth international conference on the application of stress-wave theory to piles*, Netherlands; 613-61, 1992.

[15] Rausche, F., M. Bixler, and M. Hussein, [2002]. "Non-destructive testing to determine unknown pile lengths under existing bridges," presented at the *First International Conference on Scour of Foundations*, ICSF-1; Texas Transportation Institute, College station, TX, 2002.